nature cell biology

Integrin endosomal signalling suppresses anoikis

Jonna Alanko[1,2], Anja Mai[1], Guillaume Jacquemet[1], Kristine Schauer[3], Riina Kaukonen[1], Markku Saari[1,2], Bruno Goud[3] and Johanna Ivaska[1,2,4,5]

Integrin-containing focal adhesions transmit extracellular signals across the plasma membrane to modulate cell adhesion, signalling and survival. Although integrins are known to undergo continuous endo/exocytic traffic, the potential impact of endocytic traffic on integrin-induced signals is unknown. Here, we demonstrate that integrin signalling is not restricted to cell–ECM adhesions and identify an endosomal signalling platform that supports integrin signalling away from the plasma membrane. We show that active focal adhesion kinase (FAK), an established marker of integrin–ECM downstream signalling, localizes with active integrins on endosomes. Integrin endocytosis positively regulates adhesion-induced FAK activation, which is early endosome antigen-1 and small GTPase Rab21 dependent. FAK binds directly to purified endosomes and becomes activated on them, suggesting a role for endocytosis in enhancing distinct integrin downstream signalling events. Finally, endosomal integrin signalling contributes to cancer-related processes such as anoikis resistance, anchorage independence and metastasis.

Integrins are heterodimeric cell-surface adhesion receptors functioning as integrators of the extracellular matrix (ECM)-driven cues, the cellular cytoskeleton and the cellular signalling apparatus[1]. On adhesion, integrins trigger the formation of plasma membrane-proximal large mechanosensing and signal-transmitting protein clusters depicted as 'adhesomes'[2,3]. In addition, integrins undergo constant endocytic traffic to facilitate focal adhesion turnover, cell migration, invasion and cytokinesis[4]. For other receptor systems it is well established that endocytic membrane traffic regulates bioavailability of cell-surface molecules and therefore the intensity and/or specificity of receptor-initiated signals[5,6]. Although active integrins and their ligands have been detected in endosomes[7–9] and increased integrin recycling to the plasma membrane contributes to enhanced signalling of co-trafficked receptor tyrosine kinases[10,11] it has remained unclear whether endocytosed active integrins signal in endosomes. Here, we demonstrate that integrin signalling is not restricted to focal adhesions as previously described and that endocytosis is necessary for full ECM-induced, integrin-mediated ERK, AKT and FAK signalling. We find that FAK binds directly to and can become activated on purified endosomes. Moreover, the FERM domain of FAK is able to bind purified integrin-containing endosomes, suggesting the potential for integrin-signalling complexes to assemble on endosomes after internalization of active integrins. Importantly, FAK is required for anchorage-independent growth and suppression of anoikis[12]. Integrin endosomal signalling correlates with reduced anoikis sensitivity in normal cells and anchorage-independent growth and metastasis in breast cancer cells.

RESULTS

Active FAK localizes to integrin-containing endosomes

Cell–ECM adhesion and activation of integrin signalling is necessary for cell survival, differentiation and developmental processes[13,14]. Integrin endocytosis offers an efficient system to control integrin heterodimer availability at the cell surface and thus the specific ECM-induced cellular response during processes such as cell migration and tumour cell invasion[15,16]. As FAK recruitment to focal adhesions and subsequent Tyr 397 autophosphorylation (pFAK-Y397) is an established marker of integrin–ECM engagement and downstream signalling[17] we used an anti-pFAK-Y397 antibody to visualize integrin signalling and subcellular localization in adherent cells. The pFAK-Y397 antibody detected a dominant protein band with a relative molecular mass of 125,000 in wild-type $Fak^{+/+}$ mouse embryonic fibroblasts (MEFs) that was absent in $Fak^{-/-}$ cells (Supplementary Fig. 1a) and strongly reduced on treatment with FAK inhibitors in western blots and in immunofluorescence (Supplementary Fig. 1b,c) indicative of antibody specificity towards pFAK-Y397. Immunofluorescence analyses of cells plated on micropatterns revealed that in addition to the expected ECM-interface localization of integrin and pFAK, substantial pools of both proteins could be detected within the cell body (Supplementary Fig. 1d). Analysis of

[1]Turku Centre for Biotechnology, University of Turku, Turku FIN-20520, Finland. [2]VTT Technical Research Centre of Finland, Turku FIN-20520, Finland. [3]Molecular Mechanisms of Intracellular Transport, Institut Curie, Paris 75248, France. [4]Department of Biochemistry and Food Chemistry, University of Turku, Turku FIN-20520, Finland.
[5]Correspondence should be addressed to J.I. (e-mail: johanna.ivaska@utu.fi)

Received 20 May 2015; accepted 2 September 2015; published online 5 October 2015; DOI: 10.1038/ncb3250

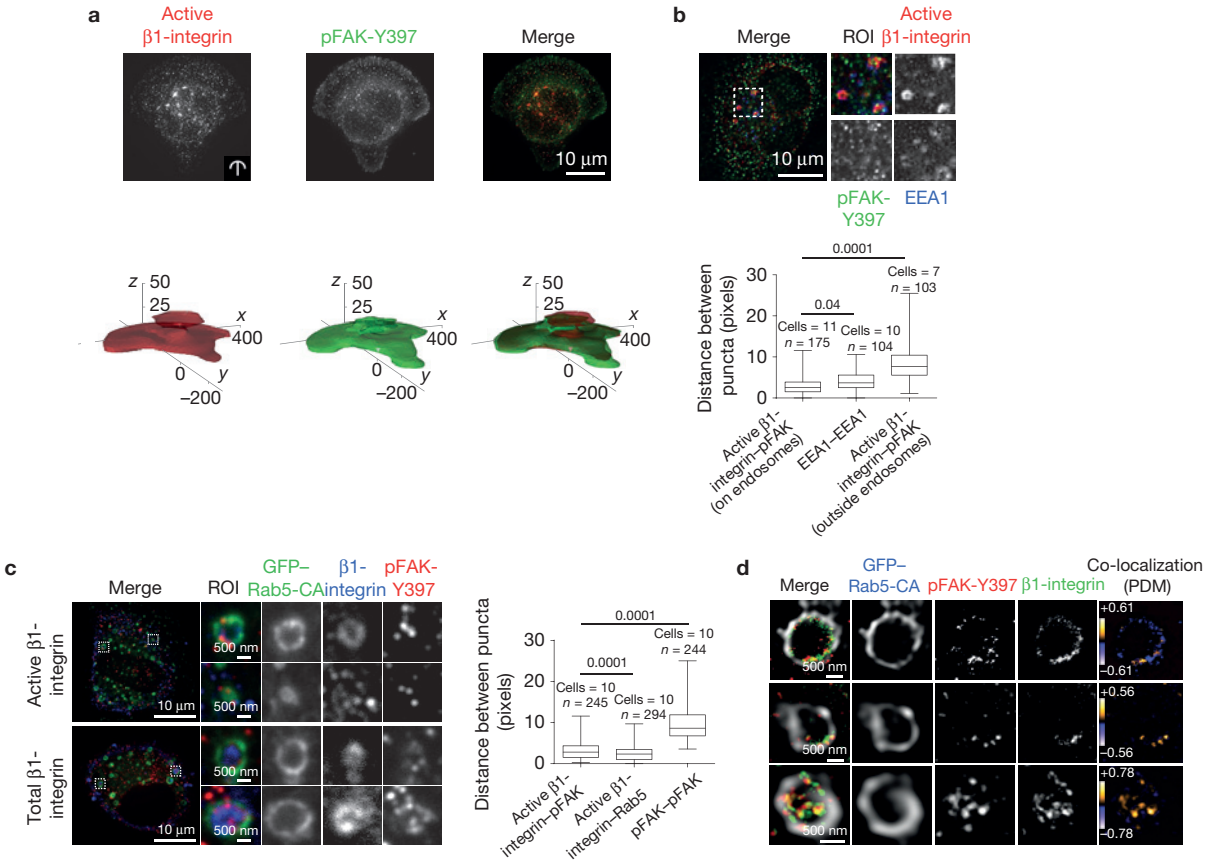

Figure 1 pFAK-Y397 localizes to endosomes together with β1-integrin. (**a**) Representative images and three-dimensional probabilistic density maps of active β1-integrin and pFAK-Y397 localization in MDA-MB-231 cells plated on crossbow-shaped fibronectin-coated micropatterns (24 cells assessed in three independent experiments). (**b**) Representative confocal images of endogenous active β1-integrin, pFAK and EEA1 staining in MDA-MB-231 cells and box plot of the distance between adjacent puncta of active β1-integrin and pFAK in or outside the EEA1-positive endosomes (in pixels; box plots show the 25th–75th percentiles delineated by the upper and lower limits of the box; the median is shown by the horizontal line inside the box; whiskers indicate maxima and minima). *n*, the number of active β1-integrin–pFAK and EEA1–EEA1 doublets (indicated in the figure) analysed from multiple cells (numbers indicated in the figure) from three independent experiments are indicated. (**c**) Representative confocal images of pFAK and total or active β1-integrin staining in GFP–Rab5-CA-expressing TIFFs adhering to fibronectin (45 min). Box plot of the distance between adjacent puncta of active β1-integrin and pFAK or Rab5 in GFP–Rab5-positive endosomes and between pFAK and pFAK outside the endosomes (in pixels; box plots show the 25th–75th percentiles delineated by the upper and lower limits of the box; the median is shown by the horizontal line inside the box; whiskers indicate maxima and minima). Numbers of cells and of active β1-integrin–pFAK, active β1-integrin–Rab5 and pFAK–pFAK doublets (*n*) analysed from three independent experiments are indicated. (**d**) Super-resolution STED images of active β1-integrin and pFAK-Y397 on single GFP–Rab5-CA endosomes in TIFFs adhering to fibronectin (45 min). Images showing PDM (product of the differences from the mean) values were generated to visualize the co-localization between β1-integrin and pFAK-Y397. ROI, region of interest. Mann–Whitney test *P* values are provided.

three-dimensional probabilistic density maps[18] of active integrin and pFAK, in which density contours represent the smallest intracellular volume containing 50% of the total immunofluorescence signal, indicated a substantial pool of pFAK at the cell centre where it overlapped with internalized active β1-integrin (9EG7 antibody; Fig. 1a). The extent of co-localization between active β1-integrin and pFAK in micropattern-normalized cells ($n = 24$) was 38.3 ± 6.2 (s.d.)%, as assessed by a particle-based analysis. A similar intracellular localization of pFAK was detected in unconstrained cells (Fig. 1b), suggesting that the non-adhesion-site-localized pFAK was not an artefact of restricting the cell geometry with micropatterns.

Exogenous expression of the constitutively active Rab5 GTPase (Rab5Q79L, Rab5-CA) results in the formation of enlarged endosome structures[19] and can be used to visualize endosomal localization of a variety of proteins, including integrins[20]. In addition, overexpression of Rab21 induces β1-integrin endocytosis and localization to enlarged early endosomes[9]. We used these properties to further investigate the subcellular localization of the intracellular active β1-integrin and pFAK. Active β1-integrin (12G10 antibody) and pFAK were visible as closely associated puncta in both Rab5-CA- and Rab21-positive endosomes in serum-starved telomerase-immortalized foreskin fibroblasts (TIFFs) actively adhering to fibronectin (Fig. 1c, Rab5CA; 98.7% and Supplementary Fig. 1e, Rab21; 97.1% of active β1-integrin-positive endosomes contained pFAK, $n = 243$ and 209 endosomes, respectively) and similar data were obtained using a total β1-integrin antibody (Fig. 1c and Supplementary Fig. 1e). Endosomal puncta of active β1-integrin and pFAK closely associated with a mean distance of ~2–3 pixels, a value similar to those obtained between active β1-integrin and Rab5 (mean distance of ~3 pixels; Fig. 1c). Similar association between active β1-integrin and pFAK was observed on early

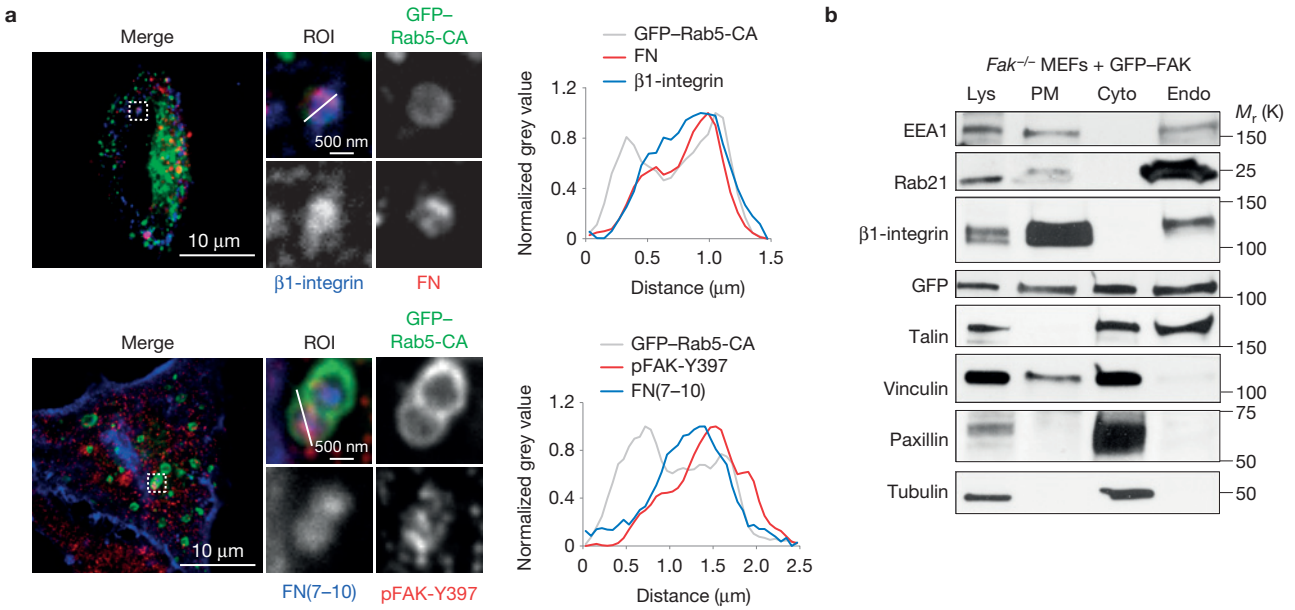

Figure 2 pFAK-Y397 localizes to endosomes together with fibronectin. (**a**) Active β1-integrin, pFAK and fibronectin localization in GFP–Rab5-CA-expressing TIFFs plated on fibronectin (top panel) or incubated with 647-labelled fibronectin fragment (FN(7–10)) for 45 min (bottom panel). Fluorescence intensity profiles (normalized grey value) across representative endosomes (solid lines) are illustrated. (**b**) Subcellular fractionation of *Fak*$^{-/-}$ MEFs re-expressing GFP–FAK and representative immunoblots from more than three independent experiments. Lys, cell lysate; PM, plasma membrane; Cyto, cytosol; Endo, endosomal fraction; ROI, region of interest. Unprocessed original scans of blots are shown in Supplementary Fig. 9.

endosome antigen-1 (EEA1)- (Fig. 1b) and Rab21-positive endosomes (Supplementary Fig. 1e). For comparison, the mean distance between randomly distributed non-endosomal pFAK and pFAK (Fig. 1c and Supplementary Fig. 1e) or active β1-integrin and pFAK outside the endosomes (Fig. 1b) was ~8–10 pixels. These puncta co-distribution analyses[21] indicate that active β1-integrin and pFAK are found in the same endosomes. Phospho-FAK recruitment to integrin-positive endosomes was further confirmed using super-resolution stimulated emission depletion (STED) microscopy (Fig. 1d). Thus, phosphorylated FAK is not restricted to focal adhesions but can also be detected on endosomes in adherent cells.

Integrin ligands and talin are present in FAK-positive endosomes

Several studies report integrin ligand localization in endosomes[8,10,22] and we have demonstrated increased endosomal retention of active β1-integrins compared with inactive receptors[7]. Importantly, we detected the integrin ligand fibronectin in pFAK and active β1-integrin-positive endosomes (Fig. 2a; 90.5% of pFAK-positive endosomes contained fibronectin, $n = 200$ endosomes), suggesting that functional receptor–ligand coupling is linked to the endosome-associated active FAK pool. Biochemical fractionations separating plasma membrane, cytoplasm and endomembrane compartments[23] demonstrated the presence of FAK in EEA1, Rab21 and β1-integrin-positive endosomal fractions (Fig. 2b). Interestingly, corresponding to the presence of active integrin receptors in endosomes, the integrin activator and focal adhesion component talin, but not paxillin and only very low levels of vinculin, was also detected in endosomes suggesting the recruitment of a specific subset of integrin adhesome proteins to endosomes.

Endocytosis contributes to integrin signalling

Next, we set out to investigate whether the endosome-associated active integrin and FAK are crucial components of integrin–ECM-induced signalling. Serum-starved cells were maintained in suspension for 1 h (to inactivate RTKs and adhesion-induced pathways) and subsequently plated on integrin ligands. Under these conditions, ECM engagement induced time-dependent activation of the canonical downstream integrin-signalling mediators including FAK, ERK1/2 and Akt without significant adhesion-dependent activation of any of the 48 different RTKs tested (Supplementary Fig. 2a,b), suggesting that the observed signals were a consequence of integrin-mediated adhesion and not due to growth factor receptor stimulation. Dynasore-mediated inhibition of dynamin[24], an important mediator of integrin receptor endocytosis[16], abrogated integrin and transferrin receptor internalization (Supplementary Fig. 3a–c) and significantly attenuated the activation of FAK and ERK1/2 in carcinoma cells and in normal fibroblasts spreading on collagen or fibronectin (Fig. 3a–d and Supplementary Fig. 4a–d) suggesting that endocytosis was key for adhesion-induced signalling. These results were recapitulated with another dynamin inhibitor Dyngo4 (ref. 25) and a dynamin dominant-negative construct (dynamin-2^{K44A}–GFP; ref. 26; Supplementary Fig. 4e,f). Interestingly, not all integrin-mediated pathways, such as Src activation, were consistently inhibited on defective dynamin function (Fig. 3a–d and Supplementary Fig. 4a–d). This may be attributed to increased integrin plasma membrane signalling supported by the slightly elevated cell-surface β1-integrin levels in dynamin-inhibited cells (Supplementary Fig. 4g). In line with these data, dynamin inhibition triggered a reduction in the *in situ* proximity ligation assay (PLA) signal between integrin and pFAK specifically in endosomes and promoted a converse increase in the plasma membrane-localized

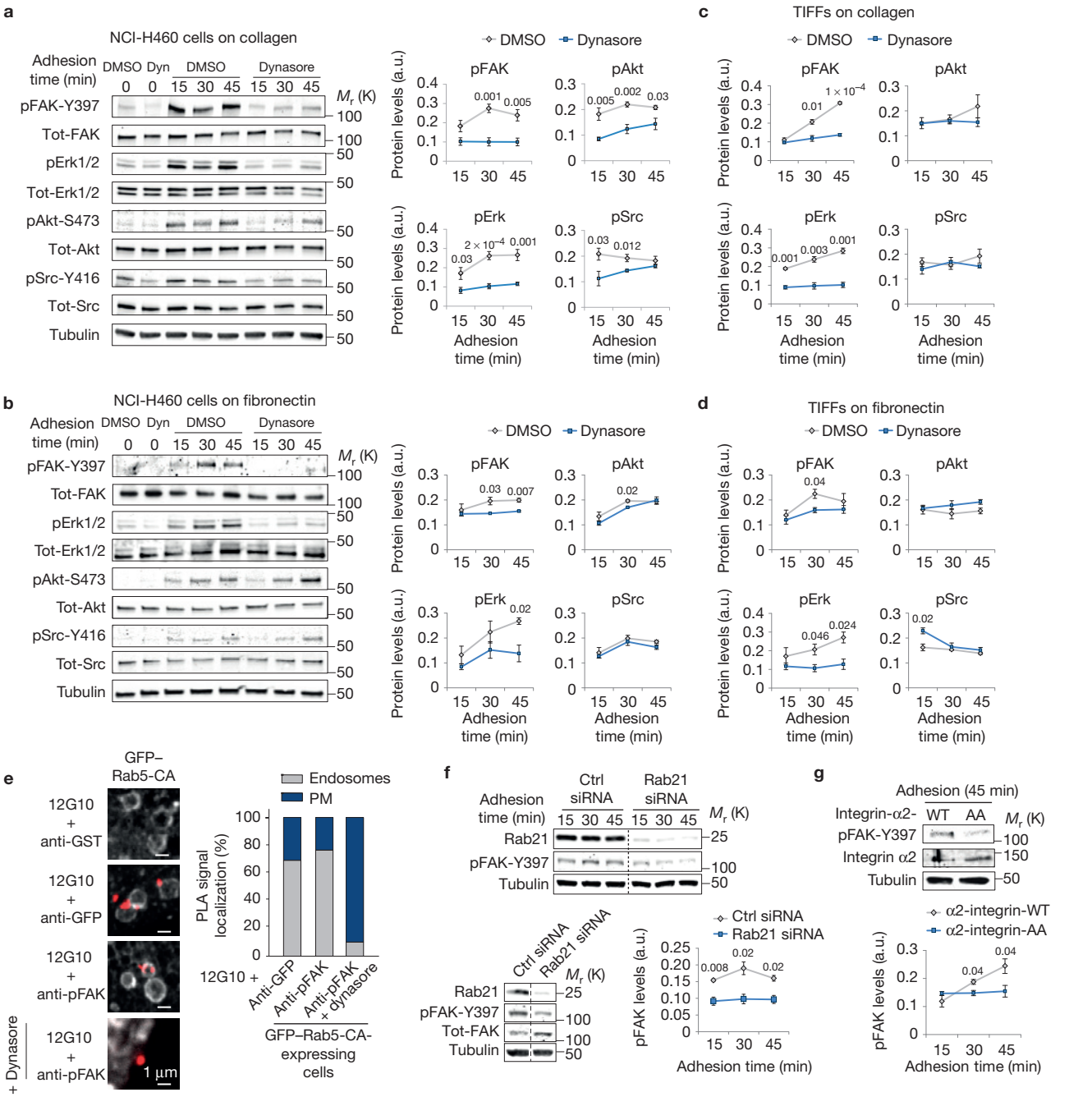

Figure 3 Inhibition of integrin endocytosis attenuates integrin signalling. (**a**–**d**) Analysis of kinase activity in NCI-H460 cells (**a**,**b**) and TIFFs (**c**,**d**) ± dynasore plated on collagen (**a**,**c**) or fibronectin (**b**,**d**) (mean ± s.e.m., (**a**) $n = 5$ independent experiments; (**b**–**d**) $n = 3$ independent experiments). (**e**) *In situ* PLA signal (red dots) representing co-localization between 12G10 (active integrin antibody) and the indicated antibodies in GFP–Rab5-CA-expressing cells (10 cells assessed from two independent experiments). (**f**) Representative immunoblot and quantification of pFAK protein levels in Rab21- or control-silenced NCI-H460 cells plated on collagen for the indicated times (mean ± s.e.m., $n = 3$ independent experiments). (**g**) Representative immunoblot and quantification of pFAK in CHO cells expressing α2-integrin wild-type (WT) or the Rab21-binding-deficient integrin α2-AA-mutant and plated on collagen for 45 min (mean ± s.e.m., $n = 3$ independent experiments). a.u., arbitrary units. Student's two-tailed unpaired *t*-test *P* values are provided and statistics source data can be found in Supplementary Table 2. Unprocessed original scans of blots are shown in Supplementary Fig. 9.

integrin–pFAK PLA signal (Fig. 3e). In addition, reduced endosomal pFAK and pAkt (another marker of downstream integrin signalling) levels, following dynasore treatment, were confirmed by subcellular fractionation (Supplementary Fig. 4h).

Integrin endosomal signalling is Rab21 dependent

As dynamin inhibition blocks several cellular endocytic routes we next used short interfering RNA (siRNA)-mediated silencing of Rab21, which interacts directly with the integrin α-subunit cytoplasmic

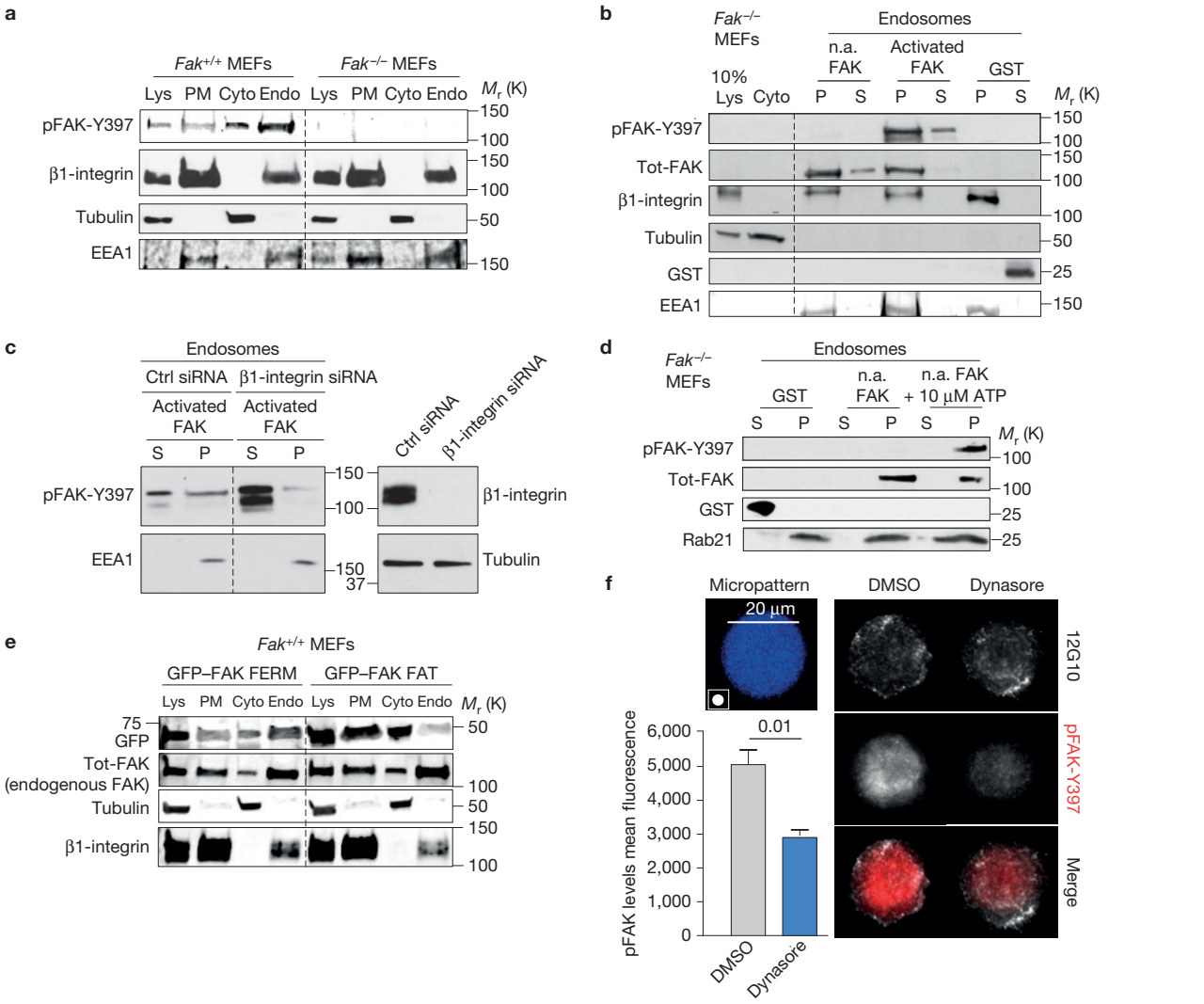

Figure 4 FAK recruitment and activation on integrin-positive endosomes. (**a**) Representative immunoblot of subcellular fractionation of *Fak*$^{+/+}$ and *Fak*$^{-/-}$ MEFs (five independent experiments). (**b**) Representative immunoblot of recombinant FAK (phosphorylated/activated or non-activated, n.a.) recruitment to insoluble endosomal pellet (P) and soluble supernatant (S) fractions isolated from *Fak*$^{-/-}$ MEFs (five independent experiments). (**c**) Representative immunoblot analysing the recruitment of recombinant FAK to purified endosomes derived from either control- or β1-integrin-silenced *Fak*$^{-/-}$ MEFs (five independent experiments). (**d**) Representative immunoblot analysing the activation of recombinant FAK in purified endosome fractions derived from *Fak*$^{-/-}$ MEFs in the presence or absence of 10 μM ATP (five independent experiments). (**e**) Subcellular fractionation of *Fak*$^{+/+}$ MEFs transfected with GFP–FAK FAT or GFP–FAK FERM. Shown are representative immunoblots of GFP–FAK fragments and endogenous FAK (total-FAK) from two independent experiments. (**f**) MDA-MB-231 cells plated on 20 μm round fibronectin-coated micropatterns (45 min) ± dynasore. Representative maximum projections and quantification of pFAK (mean fluorescence ± s.e.m., $n = 3$ independent experiments, 10 cells analysed per experiment). Lys, cell lysate; PM, plasma membrane; Cyto, cytosol; Endo, endosomal fraction. Student's two-tailed unpaired *t*-test $P = 0.01$. Unprocessed original scans of blots are shown in Supplementary Fig. 9.

tail (residues Lys 1160/Arg 1161), as a more direct mechanism to target integrin endocytosis and traffic[9,27]. RNA interference (RNAi)-mediated silencing of Rab21 (ref. 27) significantly reduced FAK phosphorylation (Fig. 3f) on matrix engagement corresponding with decreased integrin endocytosis observed in Rab21-depleted cells[9]. Furthermore, adhesion-induced signalling (pFAK levels) was significantly impaired in cells expressing an endocytosis-defective collagen-binding integrin (α2-subunit KR1160/61AA mutation as compared with wild-type α2-integrin receptor-expressing cells adhering to collagen[28] (Fig. 3g). Taken together, these data demonstrate that impaired integrin endocytosis attenuates adhesion-induced FAK activation.

FAK is recruited to and activated on purified endosomes

The requirement for endocytosis for enhanced integrin signalling could be linked to sustained signalling of plasma membrane-initiated signalling on the endosomes or the ability of integrins to trigger signalling from endomembranes. To study this further we isolated endosomes from *Fak*$^{+/+}$ and *Fak*$^{-/-}$ MEFs. β1-integrin localized to endosomal and plasma membrane fractions in both cell types indicating that integrin endosomal localization is not FAK dependent (Fig. 4a). As we found that endosomes contain a subset of integrin-signalling components (Fig. 2b) we next addressed the possibility that these components could assemble directly on the endosome.

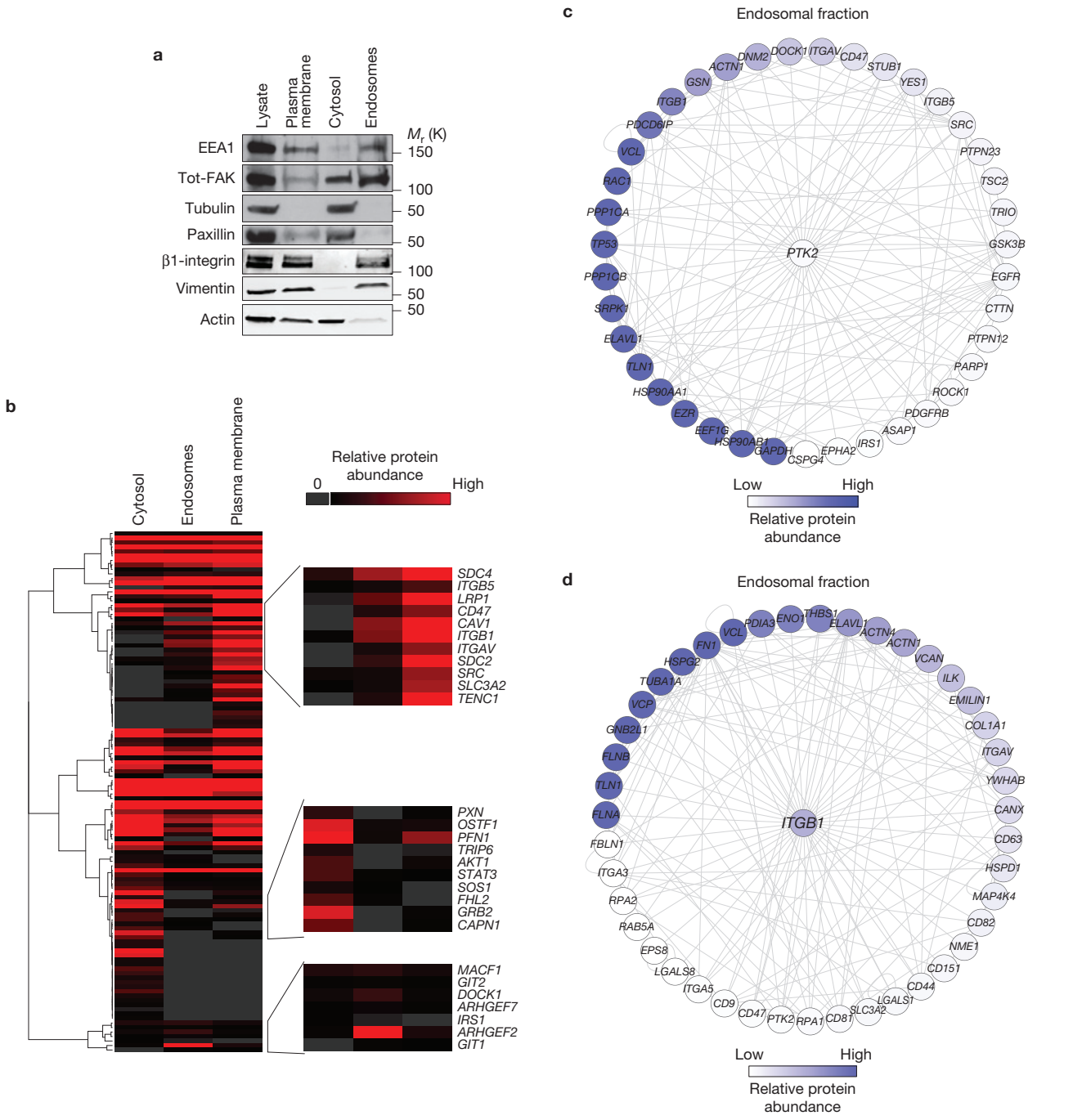

Figure 5 Endosomal proteome. (**a**) Representative western blot validation of fractionated samples analysed by mass spectrometry. (**b**–**d**) The threshold for protein identification was set at a minimum of 3 spectral counts with at least 2 unique peptides. Altogether, 2,021, 1,667 and 2,006 proteins were detected in the cytosolic, endosomal and plasma membrane fractions, respectively. (**b**) Hierarchical clustering of Geiger adhesome proteins identified in the cytoplasmic, plasma membrane and endosomal fractions. Examples of proteins detected in multiple clusters are shown on the right-hand side (two independent experiments). (**c**,**d**) Known FAK- (PTK2) (**c**) and β1-integrin- (ITGB1) (**d**) interacting proteins identified in the mass spectrometric analysis of purified endosomal fractions in *Fak*$^{+/+}$ MEFs. Proteins were mapped onto a human protein–protein interaction network. Each node represents a protein (labelled with human gene names) and each edge represents a reported interaction between two proteins. The nodes are coloured according to protein abundance (two independent experiments). Unprocessed original scans of blots are shown in Supplementary Fig. 9.

We incubated isolated integrin-containing endosomes, from *Fak*$^{-/-}$ cells, with purified recombinant FAK protein. Strikingly, soluble FAK was specifically recruited to the endosomes, independently of its phosphorylation status (Fig. 4b). Integrins contribute to this recruitment because silencing of β1-integrins reduced the amount of recruited active FAK (Fig. 4c and Supplementary Fig. 4i). Finally, the non-phosphorylated recombinant FAK became phosphorylated on Tyr 397 on the isolated endosomes *in vitro* (Fig. 4d), suggesting

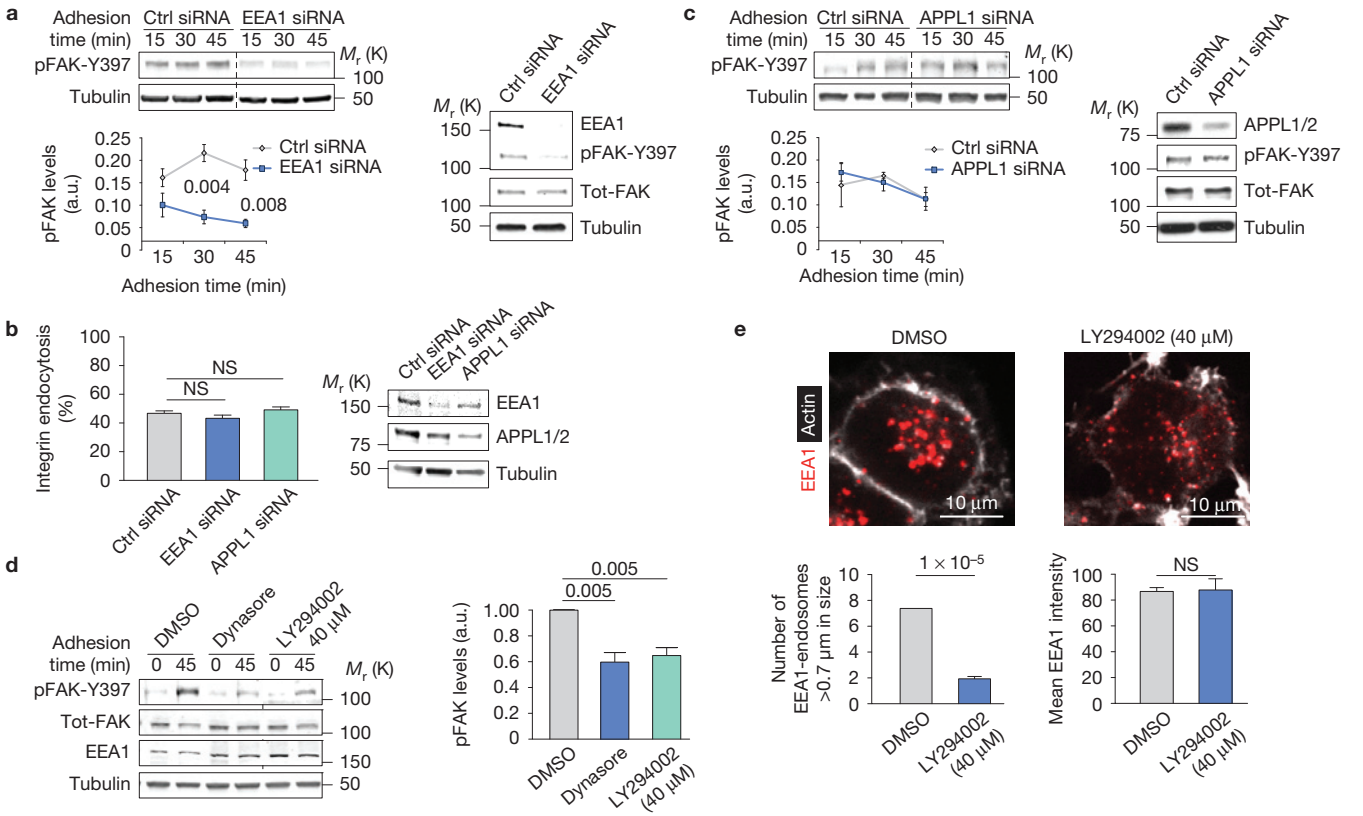

Figure 6 Integrin signalling is EEA1 dependent. (**a**) Representative blots and quantification of pFAK protein levels following EEA1 silencing in NCI-H460 cells plated on collagen (mean ± s.e.m., $n = 3$ independent experiments). (**b**) Integrin endocytosis in EEA1- or APPL1-silenced NCI-H460 cells plated on collagen (30 min) using active β1-integrin (9EG7) antibody (proportion of cytoplasmic/total staining, mean ± s.e.m., $n = 43$ cells pooled from three independent experiments). (**c**) Representative blots and quantification of pFAK protein levels following APPL1 silencing in NCI-H460 cells plated on collagen (mean ± s.e.m., $n = 3$ independent experiments). (**d**) Representative immunoblot and quantification of pFAK protein levels in NCI-H460 cells plated on collagen ± dynasore or PI(3)K inhibitor LY294002 (mean ± s.e.m., $n = 3$ independent experiments). (**e**) Representative confocal images of EEA1 and actin staining in NCI-H460 cells ± PI(3)K inhibitor (LY294002 40 μM) and quantification of the number of EEA1 endosomes larger than 0.7 μm and the total mean EEA1 intensity (mean ± s.e.m., $n = 16$ cells per condition pooled from two independent experiments). Student's two-tailed unpaired *t*-test *P* values are provided and statistics source data can be found in Supplementary Table 2. NS, not significant. Unprocessed original scans of blots are shown in Supplementary Fig. 9.

the possibility that internalized integrins could assemble endosomal signalling complexes distinct from the plasma membrane-localized adhesions. This notion was further supported by the observation that exogenous focal adhesion targeting domain of FAK alone (FAK FAT) was unable to localize to the endosomal fraction whereas the endogenous FAK and the FERM domain of FAK (FAK FERM) localized to the endosomal fraction (Fig. 4e). Taken together, these data suggest a role for endocytosis in enhancing and possibly triggering distinct integrin downstream signalling events, including FAK activation.

Integrin endocytosis is intimately coupled to the cellular cytoskeleton and cell spreading. In line with this, we observed slightly reduced cell spreading in dynasore-treated cells after 45 min of adhesion to collagen (Supplementary Fig. 5a,b). To exclude the possibility that attenuated adhesion signalling, on inhibition of integrin endocytosis, was secondary to alterations in adhesion area, we induced integrin–ECM ligation in suspension using small collagen-coated beads. Dynasore treatment significantly inhibited FAK activation on cell binding to collagen beads (Supplementary Fig. 5c), indicative of a cell spreading-independent regulatory role for endocytosis in ECM-induced integrin signalling. In addition, we found that cell adhesion to round micropatterns with restricted dimensions that constrain cell spreading supported FAK activation in an endocytosis-dependent manner (Fig. 4f).

Integrin and FAK-proximal proteins on endosomes

To gain further insight into the integrin and FAK signalling networks on the endomembranes we carried out mass spectrometric analyses of the cytoplasmic, plasma membrane and endosomal fractions of fibroblasts (Fig. 5a–d and Supplementary Table 1). Importantly, the integrin ligands fibronectin and collagen as well as many established endomembrane proteins, in addition to classic endosome markers, EHD1, Rab14 and rabaptin-5, were detected in the endosomal fraction (Fig. 5b and Supplementary Table 1). Interestingly, 69 proteins identified in the endosomal fraction are components of the literature-curated map of adhesion complexes[29] (Supplementary Table 1) and many more endosome fraction proteins were identified as adhesion components in several published mass spectrometric data sets

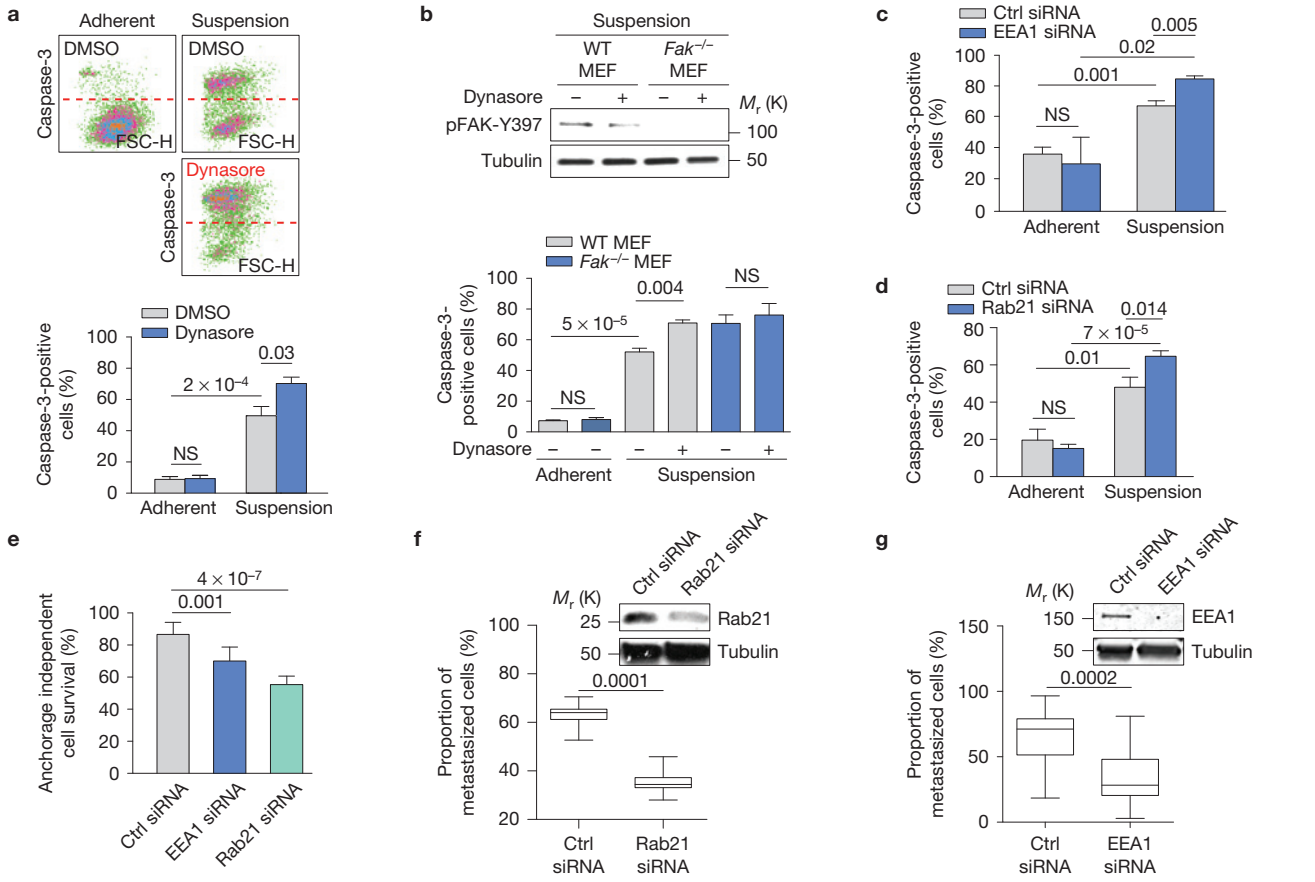

Figure 7 Integrin endosomal signalling and anoikis sensitivity are Rab21 and EEA1 dependent. (**a**–**d**) Quantification of caspase-3-positive (FL1) apoptotic cells in serum-starved TIFFs and representative dot blots (**a**), in *Fak*$^{-/-}$ or *Fak*$^{+/+}$ WT MEFs ± dynasore (**b**) and following EEA1 (**c**) or Rab21 (**d**) silencing in TIFFs (mean fluorescence ± s.e.m., $n=3$ independent experiments). (**e**) Quantification of anchorage-independent survival of MDA-MB-231 cells following EEA1 or Rab21 silencing (mean ± s.d., $n=3$ independent experiments). (**a**–**e**) Student's two-tailed unpaired *t*-test *P* values are provided. (**f**,**g**) MDA-MB-231 cells transfected with Ctrl siRNA and Rab21 siRNA (**f**) or Ctrl siRNA and EEA1 siRNA (**g**) were fluorescently labelled with green or far-red cell trackers and co-injected 1:1 into the tail vein of mice. The proportion of extravasated cells was analysed by flow cytometry 48 h after co-injection and is represented as a percentage of total extravasated cells in the lung (box plots show the 25th–75th percentiles delineated by the upper and lower limits of the box; the median is shown by the horizontal line inside the box; whiskers indicate maxima and minima; Rab21 siRNA: $n=15$ mice from one experiment, EEA1 siRNA: $n=10$ and 15 mice pooled from two independent experiments). Student's two-tailed unpaired *t*-test *P* values are provided. NS, not significant. Unprocessed original scans of blots are shown in Supplementary Fig. 9. Statistics source data can be found in Supplementary Table 2.

(Supplementary Table 1 and Methods for details). To highlight putative regulators of FAK or β1-integrin on endosomes, proteins identified in the endosomal fraction were mapped onto a human protein–protein interaction network and sub-networks containing FAK (Fig. 5c) and β1-integrin (Fig. 5d) binders were created.

The proteins in both networks have very interesting activities that are likely to contribute to integrin signalling and maintenance of receptor activity. These included actin-binding proteins, scaffolding proteins, integrin activity regulators (for example, talin), phosphatases known to contribute to signalling and several guanine nucleotide exchange factors (GEFs) implicated in the regulation of the small GTPases Rac and Rho. Interestingly, Src and paxillin, both important components of FAK signalling in focal adhesions, were not abundant in the endomembrane fraction (compared with the plasma membrane or cytosolic fractions; Fig. 5b). These data suggest that integrin signalling on endosomes may involve unique features not present in integrin signalling in focal adhesions.

Integrin endosomal signalling is EEA1 dependent

We next investigated whether increased integrin traffic could augment signalling. Transient overexpression of Rab5-CA and Rab21, previously reported to increase integrin endocytosis in multiple cell types[9,28,30], significantly promoted adhesion-dependent FAK activation (Supplementary Fig. 6a,b). Active β1-integrin and pFAK are present on endosomes positive for endogenous EEA1, a key Rab5 effector[31,32], associated with both Rab5- and Rab21-positive endosomes[4] (Fig. 1c and Supplementary Fig. 1e) and EEA1 and pFAK localize to GFP–EEA1-positive endosomes in fibroblasts adhering to fibronectin (Supplementary Fig. 6c). Although multiple endosomal signalling pathways are EEA1 dependent, a second class of Rab5-positive, EEA1-negative early endosomes containing one or both of the closely related APPL1 and APPL2 adaptors have also been implicated in signalling[33–35]. Silencing of EEA1 with a single siRNA oligonucleotide (Fig. 6a) or an independent siRNA smart pool (Supplementary Fig. 6d) significantly reduced adhesion-induced

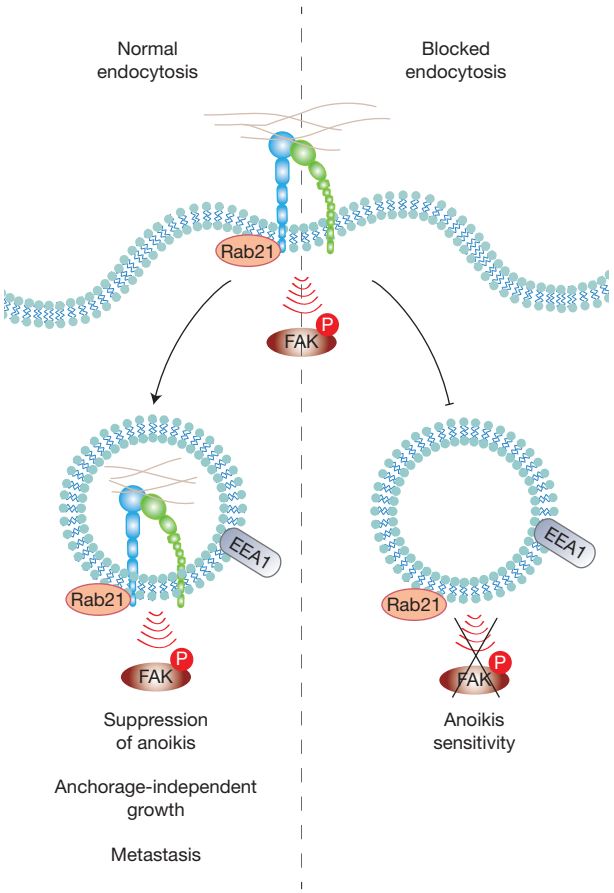

Figure 8 Conclusion model showing the role of adhesion-induced integrin endosomal signalling in the regulation of anoikis. The full activation of the ECM-induced integrin pFAK-Y397 signal is dependent on Rab21-mediated integrin endocytosis to EEA1-containing early endosomes, and this is ultimately required for suppression of anoikis and anchorage-independent growth. Blocked integrin endocytosis leads to reduced FAK activation and to increased anoikis sensitivity.

FAK activation (Fig. 6a) without influencing integrin endocytosis (Fig. 6b). In contrast, silencing of APPL1 had no effect on integrin signalling or endocytosis in response to adhesion (Fig. 6b,c). The recruitment of EEA1 to endosomes requires the generation of phosphatidylinositol 3-phosphate (PI(3)P) and inhibition of phosphoinositide-3-phosphate kinase (PI(3)K) has been shown to decrease the number of EEA1-containing endosomes while increasing the size of APPL1-positive vesicles[36]. Accordingly, treatment of cells with a PI(3)K inhibitor triggered a reduction in the number of EEA1-positive endosomes without reducing total EEA1 levels and inhibited adhesion-induced FAK activation similarly to dynasore treatment (Fig. 6d,e). Taken together, our results reveal an important role for EEA1 but not APPL1 in integrin endosomal signalling.

Integrin endosomal signalling inhibits anoikis

A central function for integrin-induced signalling is adhesion-dependent cell survival. On detachment, normal cells undergo a specialized form of programmed cell death called anoikis, and canonical integrin-mediated activation of FAK on the plasma membrane has been considered critical for anoikis suppression[12]. On detachment, serum-starved fibroblasts exhibited relatively fast anoikis and inhibition of integrin endocytosis with dynasore or Dyngo4a significantly increased the fraction of apoptotic cells 5 h post detachment but had no effect on cell survival in adherent cells (Fig. 7a and Supplementary Fig. 7a). Importantly, dynasore treatment reduced pFAK and induced anoikis sensitivity in $Fak^{+/+}$ MEFs in suspension to levels seen in $Fak^{-/-}$ MEFs under the same experimental condition; however, dynamin inhibition did not further increase apoptosis in $Fak^{-/-}$ MEFs (Fig. 7b), indicative of a link between FAK activation and sensitivity to dynasore-induced anoikis. Finally, because EEA1 endosomes (but not APPL endosomes) and Rab21-mediated endocytosis were identified as critical contributors to integrin endosomal FAK signalling (Figs 3h and 2f), we tested the effect of EEA1, APPL-1 and Rab21 silencing on anoikis sensitivity. RNAi transfections increased the proportion of apoptotic cells to some extent in all siRNA-transfected adherent cells (Fig. 4d,e). However, on cell detachment EEA1- and Rab21-silenced cells showed significantly higher anoikis sensitivity and reduced pFAK levels (Figs 7c,d, 6a and 3f), whereas APPL1 silencing did not significantly increase anoikis (Supplementary Fig. 7b). Next we tested whether impairment of integrin signalling from endosomes negatively affects the ability of anoikis-resistant cells to grow in an anchorage-independent manner, which is a critical hallmark of cancer. We found that anchorage-independent growth of tumorigenic MDA-MB-231 cells was sensitive to FAK and dynamin inhibition (Supplementary Fig. 8a), suggesting the suitability of these cells for investigation of the functional contribution of endosomal FAK signalling. *In vitro*, silencing of EEA1 and even more significantly silencing of Rab21 reduced the proportion of live cells in suspension cultures (Fig. 7e). As anchorage-independent growth has been linked to metastasis[37], we investigated the ability of MDA-MB-231 cells to survive in vasculature and metastasize to lungs. When control and Rab21 siRNA- or control and EEA1 siRNA-transfected cells were co-injected into the same recipient animals, the number of extravasated Rab21-silenced cells in the lung tissue was significantly lower after 48 h (Fig. 7f,g and Supplementary Fig. 8b). Thus, impaired integrin endosomal signalling sensitizes cancer cells to detachment-induced cell death and impairs their metastatic potential *in vivo*.

DISCUSSION

Our study provides evidence, using multiple complementary approaches, for non-canonical β1-integrin signalling that is distinct from the signalling role of integrins in adhesion sites at the plasma membrane (Fig. 8). Our data indicate that active integrins bound to their ligands co-localize with active FAK in endosomes away from the plasma membrane. Integrin-positive endosomes contain talin, which may function to keep the integrin active. In addition, several other signalling and scaffolding proteins are detected in the isolated endosomal fraction and their functional contribution to integrin endosomal signalling will be interesting to investigate in detail in the future. We find that integrin-containing endosomes harbour the capacity to recruit and activate soluble FAK suggesting that a subset of integrin-associated proteins, present in cell–ECM adhesions, may form the core integrin-signalling platform in endosomes. It is also possible that active phosphorylated FAK is co-endocytosed with integrin receptors from the plasma membrane and that additional pFAK recruitment to the endosome acts to reinforce signalling

downstream of integrin–ECM engagement. Differentiating between these two distinct mechanisms, co-endocytosis or reassembly of integrin-signalling complexes at the endosome, will be crucial for our understanding of integrin endosomal signalling and will require further comprehensive investigation. Nevertheless, integrin signalling from EEA1 endosomes, revealed in this study, functions to accentuate adhesion-induced signalling and facilitates extended survival in anoikis-sensitive cells. Interestingly, the targeting of FAK to endosomes seems to be distinct from its focal adhesion recruitment[38]. The FAT sequence in FAK is sufficient alone to localize to focal adhesions in cells; however, we find that localization to the endosomes is mediated by the FAK FERM domain and not the FAT domain. Furthermore, Src, which is a critical enhancer of FAK activity and its downstream signalling in focal adhesions[39], is only very weakly detectable in the integrin-containing endosomal fractions. Thus, targeting and activation of FAK on endosomes may be mechanistically distinct from its regulation in focal adhesions.

We show here that endosome-localized active integrin and FAK signalling contribute to cancer-related processes such as anchorage-independent growth and metastasis. In the future, unravelling mechanisms involved in the endosomal activation of FAK in non-adherent cells may uncover possible therapeutic targets in anoikis-resistant transformed cells. □

METHODS

Methods and any associated references are available in the online version of the paper.

Note: Supplementary Information is available in the online version of the paper

ACKNOWLEDGEMENTS

We thank J. Siivonen and P. Laasola for excellent technical assistance, M. Georgiadou, D. Schlaepfer and J. Heino for insightful comments on the manuscript and H. Hamidi for scientific writing and editing of the manuscript. S. Corvera is acknowledged for the GFP–EEA1 plasmid (Addgene), D. Schlaepfer for the FAK wt and −/− MEFs and the GFP–FAK plasmids, T. Näreoja and S. Koho for assistance with the STED instrument, and Cell Imaging Core facility, University of Turku Centre for Biotechnology, and the Nikon Imaging Centre at Institut Curie-CNRS for help with the imaging. Turku Centre for Disease Modelling is acknowledged for help with the metastasis assays. This study has been supported by the Academy of Finland, ERC Starting Grant, ERC Consolidator Grant, the Sigrid Juselius Foundation, and the Finnish Cancer Organization. J.A. has been supported by the Turku Doctoral Program of Biomedical Sciences and an EMBO Short-Term Fellowship. G.J. is supported by an EMBO Long-Term Fellowship.

AUTHOR CONTRIBUTIONS

J.I. conceived and supervised the study, carried out experiments, analysed the data and wrote the manuscript with the contribution of J.A., B.G. and A.M. K.S. and B.G. supervised and helped analyse micropatterning experiments and gave helpful insights and discussion. J.A. designed, carried out and analysed most of the experiments with crucial help from A.M., R.K. and M.S. G.J. and A.M. designed, carried out and analysed the mass spectrometry experiments.

COMPETING FINANCIAL INTERESTS

The authors declare no competing financial interests.

Published online at http://dx.doi.org/10.1038/ncb3250
Reprints and permissions information is available online at www.nature.com/reprints

1. Harburger, D. S. & Calderwood, D. A. Integrin signalling at a glance. *J. Cell. Sci.* **122,** 159–163 (2009).
2. Winograd-Katz, S. E., Fassler, R., Geiger, B. & Legate, K. R. The integrin adhesome: from genes and proteins to human disease. *Nat. Rev. Mol. Cell Biol.* **15,** 273–288 (2014).
3. Zaidel-Bar, R., Itzkovitz, S., Ma'ayan, A., Iyengar, R. & Geiger, B. Functional atlas of the integrin adhesome. *Nat. Cell Biol.* **9,** 858–867 (2007).
4. De Franceschi, N., Hamidi, H., Alanko, J., Sahgal, P. & Ivaska, J. Integrin traffic—the update. *J. Cell. Sci.* **128,** 839–852 (2015).
5. Ceresa, B. P. & Schmid, S. L. Regulation of signal transduction by endocytosis. *Curr. Opin. Cell Biol.* **12,** 204–210 (2000).
6. Scita, G. & Di Fiore, P. P. The endocytic matrix. *Nature* **463,** 464–473 (2010).
7. Arjonen, A., Alanko, J., Veltel, S. & Ivaska, J. Distinct recycling of active and inactive β1 integrins. *Traffic* **13,** 610–625 (2012).
8. Dozynkiewicz, M. A. *et al.* Rab25 and CLIC3 collaborate to promote integrin recycling from late endosomes/lysosomes and drive cancer progression. *Dev. Cell* **22,** 131–145 (2012).
9. Pellinen, T. *et al.* Small GTPase Rab21 regulates cell adhesion and controls endosomal traffic of β1-integrins. *J. Cell Biol.* **173,** 767–780 (2006).
10. Muller, P. A. *et al.* Mutant p53 drives invasion by promoting integrin recycling. *Cell* **139,** 1327–1341 (2009).
11. Muller, P. A. *et al.* Mutant p53 enhances MET trafficking and signalling to drive cell scattering and invasion. *Oncogene* **32,** 1252–1265 (2013).
12. Frisch, S. M., Vuori, K., Ruoslahti, E. & Chan-Hui, P. Y. Control of adhesion-dependent cell survival by focal adhesion kinase. *J. Cell Biol.* **134,** 793–799 (1996).
13. Geiger, B., Bershadsky, A., Pankov, R. & Yamada, K. M. Transmembrane crosstalk between the extracellular matrix–cytoskeleton crosstalk. *Nat. Rev. Mol. Cell Biol.* **2,** 793–805 (2001).
14. Hynes, R. O. The extracellular matrix: not just pretty fibrils. *Science* **326,** 1216–1219 (2009).
15. Bridgewater, R. E., Norman, J. C. & Caswell, P. T. Integrin trafficking at a glance. *J. Cell. Sci.* **125,** 3695–3701 (2012).
16. Caswell, P. T., Vadrevu, S. & Norman, J. C. Integrins: masters and slaves of endocytic transport. *Nat. Rev. Mol. Cell Biol.* **10,** 843–853 (2009).
17. Brunton, V. G. & Frame, M. C. Src and focal adhesion kinase as therapeutic targets in cancer. *Curr. Opin. Pharmacol.* **8,** 427–432 (2008).
18. Schauer, K. *et al.* Probabilistic density maps to study global endomembrane organization. *Nat. Methods* **7,** 560–566 (2010).
19. Stenmark, H. *et al.* Inhibition of rab5 GTPase activity stimulates membrane fusion in endocytosis. *EMBO J.* **13,** 1287–1296 (1994).
20. Lobert, V. H. *et al.* Ubiquitination of α 5 β 1 integrin controls fibroblast migration through lysosomal degradation of fibronectin-integrin complexes. *Dev. Cell* **19,** 148–159 (2010).
21. Monteiro, P. *et al.* Endosomal WASH and exocyst complexes control exocytosis of MT1-MMP at invadopodia. *J. Cell Biol.* **203,** 1063–1079 (2013).
22. Christoforides, C., Rainero, E., Brown, K. K., Norman, J. C. & Toker, A. PKD controls αvβ3 integrin recycling and tumor cell invasive migration through its substrate Rabaptin-5. *Dev. Cell* **23,** 560–572 (2012).
23. Bass, M. D. *et al.* A syndecan-4 hair trigger initiates wound healing through caveolin- and RhoG-regulated integrin endocytosis. *Dev. Cell* **21,** 681–693 (2011).
24. Kirchhausen, T., Macia, E. & Pelish, H. E. Use of dynasore, the small molecule inhibitor of dynamin, in the regulation of endocytosis. *Methods Enzymol.* **438,** 77–93 (2008).
25. Hill, T. A. *et al.* Inhibition of dynamin mediated endocytosis by the dynoles—synthesis and functional activity of a family of indoles. *J. Med. Chem.* **52,** 3762–3773 (2009).
26. Damke, H., Baba, T., Warnock, D. E. & Schmid, S. L. Induction of mutant dynamin specifically blocks endocytic coated vesicle formation. *J. Cell Biol.* **127,** 915–934 (1994).
27. Mai, A. *et al.* Competitive binding of Rab21 and p120RasGAP to integrins regulates receptor traffic and migration. *J. Cell Biol.* **194,** 291–306 (2011).
28. Pellinen, T. *et al.* Integrin trafficking regulated by Rab21 is necessary for cytokinesis. *Dev. Cell* **15,** 371–385 (2008).
29. Zaidel-Bar, R. & Geiger, B. The switchable integrin adhesome. *J. Cell. Sci.* **123,** 1385–1388 (2010).
30. Sandri, C. *et al.* The R-Ras/RIN2/Rab5 complex controls endothelial cell adhesion and morphogenesis via active integrin endocytosis and Rac signaling. *Cell Res.* **22,** 1479–1501 (2012).
31. Mu, F. T. *et al.* EEA1, an early endosome-associated protein. EEA1 is a conserved α-helical peripheral membrane protein flanked by cysteine "fingers" and contains a calmodulin-binding IQ motif. *J. Biol. Chem.* **270,** 13503–13511 (1995).
32. Christoforidis, S., McBride, H. M., Burgoyne, R. D. & Zerial, M. The Rab5 effector EEA1 is a core component of endosome docking. *Nature* **397,** 621–625 (1999).
33. Erdmann, K. S. *et al.* A role of the Lowe syndrome protein OCRL in early steps of the endocytic pathway. *Dev. Cell* **13,** 377–390 (2007).
34. Miaczynska, M. *et al.* APPL proteins link Rab5 to nuclear signal transduction via an endosomal compartment. *Cell* **116,** 445–456 (2004).
35. Miaczynska, M., Pelkmans, L. & Zerial, M. Not just a sink: endosomes in control of signal transduction. *Curr. Opin. Cell Biol.* **16,** 400–406 (2004).
36. Zoncu, R. *et al.* A phosphoinositide switch controls the maturation and signaling properties of APPL endosomes. *Cell* **136,** 1110–1121 (2009).
37. Paoli, P., Giannoni, E. & Chiarugi, P. Anoikis molecular pathways and its role in cancer progression. *Biochim. Biophys. Acta* **1833,** 3481–3498 (2013).
38. Prutzman, K. C. *et al.* The focal adhesion targeting domain of focal adhesion kinase contains a hinge region that modulates tyrosine 926 phosphorylation. *Structure* **12,** 881–891 (2004).
39. Owen, J. D., Ruest, P. J., Fry, D. W. & Hanks, S. K. Induced focal adhesion kinase (FAK) expression in FAK-null cells enhances cell spreading and migration requiring both auto- and activation loop phosphorylation sites and inhibits adhesion-dependent tyrosine phosphorylation of Pyk2. *Mol. Cell. Biol.* **19,** 4806–4818 (1999).

METHODS

Cells. The following cell lines were used in this study: MDA-MB-231 (human breast adenocarcinoma) maintained in DMEM containing 1% MEM non-essential amino acids, 1% L-glutamine and 10% fetal bovine serum (FBS); NCI-H460 (human non-small cell lung carcinoma) in RPMI-1640 (R5886 Sigma) containing 10% FBS, 1% L-glutamine, 1% sodium pyruvate, 1% HEPES (1 M) and 1% glucose (45%); TIFFs (human telomerase-immortalized foreskin fibroblasts, a gift from J. Norman, The Beatson Institute for Cancer Research, Glasgow, UK) maintained in DMEM containing 1% L-glutamine, 2% HEPES (1 M) and 20% FBS; CHO (Chinese hamster ovary cells) in Alpha-MEM (M4526, Sigma) containing 1% L-glutamine and 5% FBS; GD25-β1A (mouse fibroblasts, described in ref. 40) cultured in DMEM containing 1% L-glutamine, 10% FBS and 10 μg ml^{-1} puromycin and *Fak*$^{-/-}$ and *Fak*$^{+/+}$ MEFs (mouse embryonic fibroblasts provided by D. Schlaepfer, UCSF, USA, described in ref. 41) cultured in DMEM containing 10% FBS, 100 U ml^{-1} penicillin, 100 μg ml^{-1} streptomycin, 1% MEM non-essential amino acids, 1% sodium pyruvate and 1% L-glutamine. DMEM was from Sigma (D5796). Unless otherwise indicated, the cell lines were obtained from American Type Culture Collection (ATCC). The cell lines used in this study are not found in the ICLAC database for cross-contaminated or otherwise misidentified cell lines, and were not authenticated. All cells were serum starved for 24 h before all experiments unless otherwise indicated. All cells were routinely tested for mycoplasma contamination. All experiments were repeated at least three times unless otherwise indicated.

Antibodies and reagents. A detailed list of used primary antibodies is provided in Supplementary Table 3. Phalloidin–Atto 647N (65906-10NMOL) was purchased from Fluka; AlexaFluor-conjugated secondary antibodies (488, 555, 647-conjugated anti-mouse, rabbit and rat antibodies) were purchased from Life Technologies; Mega-520 (rabbit) and Atto-647 (mouse) secondary antibodies for STED were from Sigma; secondary antibodies for detecting immunoblots with Odyssey (DyLight 680- and 800-conjugated anti-mouse, rabbit and rat antibodies) were from Thermo Scientific. Live-cell dyes, Far-red DDAO-SE and green CMFDA were obtained from Molecular Probes. Dynasore monohydrate (D7693), dimethylsulphoxide (DMSO; D2650) and collagen type I solution (C8919) were obtained from Sigma. Dyngo4a was from Abcam (ab120689) and FAK inhibitors PF-562271 (S2890) and PF-573228 (S2013) were obtained from Selleckchem. The CellPlayer 96-Well Kinetic Caspase-3/7 Apoptosis Assay Kit (Nucview, 4440) was purchased from Essen Bioscience, LY294002 (PHZ1144) and AlexaFluor568-conjugated transferrin (T-23365) from Life Technologies, fibronectin bovine plasma (341631) from Merck and Polybead Microspheres 6.00 μm (07312-5) from Polysciences. FAK inhibitor 14 (3414) and Human Phospho-RTK Array (ARY001) were from R&D Systems. Active (0165-0000-3) and non-activated (0165-0000-1) recombinant FAK were purchased from ProQinase. pET15b-FNIII (7-10) was a gift from R. Fässler (MPI of Biochemistry, Martinsried, Germany). HyQTase (SV30030.01) from HyClone was used to detach cells for replating before the start of the experiment.

siRNAs and plasmids. The following siRNAs and their target sequences were used (all from Qiagen): Allstars negative control siRNA (1027281); EEA1 siRNA, 5′-ATGGATAACATGACCTTGGAA-3′; EEA1 smart pool (three siRNAs), 5′-AGCCGCTATATTAGACTTGGA-3′, 5′-AAGCTAAGTTGCATTCCGAAA-3′, 5′-CCCGGCACAGAATGTGAGTTA-3′; β1-integrin siRNA, 5′-CCCGACATCATCCCAATTGTA-3′, and 5′-CTGGTCCATGTCTAGCGTCAA-3′; Rab21 siRNA, 5′-AAGGCATCATTCTTAACAAAG-3′ (3′-AlexaFluor555); and APPL1 siRNA, 5′-CAGGACAATCTCGGCCACCGA-3′. The following plasmids were used: pEGFP-C1 (Clontech), GFP–Rab5-Q79L and GFP–Rab21 (ref. 9), pIRES-GFP-α2 WT/-α2-AA (ref. 28), GFP–Dyn2K44A (ref. 42), GFP–EEA1 (Addgene plasmid 42307; ref. 43), GFP–FAK wt, GFP–FAK FERM (1–402) and GFP–FAK FAT from D. Schlaepfer. Lipofectamine 2000 (11668-019, Life Technologies) and HiPerfect (301705, Qiagen) were used for transient transfections and siRNA silencing according to the manufacturer's protocol.

Subcellular fractionation. The protocol was modified from ref. 23. Briefly, adherent cells were scraped on ice into hypotonic lysis buffer (10 mM HEPES-KOH pH 7.2, 0.25 M sucrose, 1 mM EDTA, 1 mM MgOAc and protease and phosphatase inhibitors (PhosSTOP and Complete mini tablets from Roche)). Cell membranes were fragmented with a French press and nuclei removed with 10 min 1,000*g* centrifugation. The plasma membrane fraction was collected with 10 min 10,000*g* centrifugation and endosomal/cytoplasmic fractions with 1 h 100,000*g* centrifugation. Membrane fractions were washed at least once with lysis buffer and cytoplasmic fractions were centrifuged twice. All fractionation steps were performed at +4 °C or on ice. All fractions were dissolved in sample buffer for immunoblotting. Direct protein binding to isolated endosomes was assessed with recombinant proteins. Therefore, the endosomal fraction derived from *Fak*$^{-/-}$ MEFs was resuspended in buffer containing 20 mM Tris-HCl pH 7.4, 150 mM NaCl, 1 mM $MgCl_2$, 1 mM dithiothreitol and protease and phosphatase inhibitors and subsequently incubated with 0.5 μg of either phosphorylated or non-phosphorylated FAK (ProQinase) or GST for 2 h at room temperature. To assess whether FAK can be activated on endosomes *in vitro*, GST or non-phosphorylated FAK was incubated for 1.5 h with the purified endosomes and then 10 μM ATP was added or not for another 30 min. Following 100,000*g* centrifugation for 1 h, the total soluble (supernatant) and non-soluble endosomal (pellet) fractions were analysed by SDS–PAGE followed by western blotting with the indicated antibodies.

***In situ* proximity ligation assay (PLA).** PLA was done according to the manufacturer's protocol (Duolink, Olink BioScience) in serum-starved TIFFs plated on collagen for 45 min ± dynasore followed by 4% PFA + 1 mM $MgCl_2$ fixing.

Replating assay. The same protocol was used in all experiments where integrin signalling was activated by integrin ligand engagement at different time points. Cells were serum starved for 24 h, detached with HyQTase, washed and kept in suspension in serum-free medium for 1 h to stop adhesion signalling. Dynasore (80 μM; refs 44,45), LY294002 (40 μM), Dyngo4a (10 μM) or equal volumes of DMSO were added to cells 15 min before replating on collagen type I or fibronectin-coated (5 μg ml^{-1}) dishes or coverslips for different time points at +37 °C. Cells were washed with cold PBS and collected on ice for immunoblotting.

Inhibitor assay. Adherent unstarved cells were treated with FAK inhibitors (10 μM of FAK-14, 1 μM of PF271 or 1 μM of PF228) for 3 h at +37 °C after which the cells were either fixed and stained for immunofluorescence or collected in sample buffer for immunoblotting.

Immunoblotting. Immunoblotting was performed by using standard western blotting techniques and either an ECL detection or Odyssey LICOR imaging system. The level of phosphorylated proteins was quantified by measuring the integrated band intensities with NIH ImageJ (1.45 s) and unless otherwise indicated, band intensities of phospho-proteins were normalized to the corresponding tubulin band and to the sum of all time points inside an experiment.

Flow cytometric assay. Cells were treated as described for the replating assay with the exception that in the end cells were detached with HyQTase, washed and fixed. Fixing and staining of the cells was performed as described in ref. 46.

Bead assay. Beads (6 μm, Polybead Microspheres) were coated with 10 μg ml^{-1} collagen in 2% BSA for 2 h at +37 °C and blocked with 2% BSA/PBS for 1 h at room temperature. Serum-starved cells were treated with DMSO or dynasore as described in the replating assays, mixed with coated beads in low-attachment 6-well cell culture dishes (Corning Costar Ultra-Low attachment 6-well plate, CLS3471, Corning) and incubated at +37 °C for 45 min. Cold PBS was added to the wells, and cells with beads were collected on ice, centrifuged at 210*g* for 3 min at +4 °C and resuspended in sample buffer for immunoblotting.

Anoikis assay. Adherent, serum-starved cells were treated with 80 μM dynasore, 3 or 10 μM Dyngo4a or equivalent amounts of DMSO for 1 h at +37 °C. Cells were maintained at +37 °C for 5 h or detached with HyQTase, washed and suspended in 5 ml of serum-free medium containing the same concentrations of dynasore or Dyngo4a and kept in suspension for 5 h at +37 °C. Adherent cells were collected with HyQTase and all cells were then analysed for caspase-3/7 positivity using the Nucview Apoptosis Assay according to the manufacturer's protocol (Essen Bioscience).

Immunofluorescence, microscopy, image and co-distribution analysis. Cells plated on Ibidi dishes (Integrated Biodiagnostics) or on acid-washed coverslips were fixed with 4% paraformaldehyde (PFA) containing 1 mm $MgCl_2$ for 15 min at room temperature and permeabilized with 0.2% Triton X-100 in 30% horse serum/TBS for 15 min at room temperature. Samples were blocked and antibodies were diluted in 30% horse serum/TBS. Primary antibodies were used at predetermined concentrations (5–10 μg ml^{-1}) and AlexaFluor secondary antibodies as 5 μg ml^{-1}. Unless otherwise stated, all images were acquired using the spinning-disc confocal microscope as described previously[7] with the exception of a 100×/1.3 Oil (Pha3, EC Plan Neofluar) objective being used. The microscope, image acquisition and related data analysis for the crossbow-shaped micropatterns are described in ref. 18. Quantitative analysis for all other images was performed using NIH ImageJ (1.45 s). Following background subtraction, β1-integrin and 555-Trf endocytosis was calculated from mid-slices by measuring the integrated density within the cell as a percentage of the total integrated density (integrin endocytosis) or by measuring the mean intensity of the cell (Trf endocytosis). A Leica TCS SP5 stimulated emission depletion (STED) laser scanning microscope was used to acquire images at the super-resolution level (Leica Microsystems GmbH), where approximately 65 nm resolution in the x, y axis was achieved. A Leica STED infrared-corrected objective

DOI: 10.1038/ncb3250

100×/1.4 was used. Mega-520 fluorophore was excited at 532 nm wavelength (PicoQuant) and Star-635 at 635 nm wavelength (PicoQuant). The channels were scanned sequentially and emission was detected by avalanche photodiode detectors at the emission range of 685/40 (Leica Microsystems GmbH). Leica LAS software (Leica Microsystems GmabH) was used to perform background subtraction and deconvolution in all images. In the deconvolution process a Lorentzian point spread function (PSF) was generated by using the measured PSF value of 62 nm, which was exploited to signal energy based deconvolution algorithm. Deconvolution was done by using the deconvolution tool box included in Leica LAS imaging software. GFP–Rab5-CA was imaged with confocal resolution, by using a 488 nm laser line for excitation, and emission was detected at 500–530 nm. In the deconvolution process a Gaussian PSF was generated for the confocal channel by using the measured PSF value of 230 nm, which was exploited to signal energy based deconvolution algorithm. STED imaging was performed at the Laboratory of Biophysics, University of Turku. Image co-localization analysis was performed by using the Intensity Correlation Analysis plugin for ImageJ to create PDM (product of the differences from the mean) images, where PDM = (red intensity − mean red intensity) × (green intensity − mean green intensity). Analysis of co-distribution between active β1-integrin and pFAK puncta on microdomains of either Rab5-, Rab21- or EEA1-positive endosomes was performed as described in ref. 15. The distance between pFAK and FAK was measured by selecting a random non-endosomal pFAK puncta and measuring the distance to the closest neighbour pFAK puncta.

Micropatterns and probabilistic density maps. Micropatterns were produced on glass coverslips as described in ref. 47. Cells were seeded on micropatterns in serum-free medium for either 3 h or 45 min (cells on spots) before fixing. Samples were stained as described above. The microscope, image acquisition and creation of the probabilistic density maps are described in ref. 18.

Mice. Eight-week-old female Hsd:Athymic Nude–Foxn1nu mice were used for animal experiments. Studies were performed under a valid animal licence (licence number 4199/04.10.07/2014) and conducted according to the Finnish act on animal experimentation guidelines.

Lung extravasation. Control and Rab21 or EEA1 siRNA-transfected MDA-MB-231 cells were labelled with live-cell dyes (Ctrl siRNA: Far-red DDAO-SE; Rab21 siRNA/EEA1 siRNA: green CMFDA) according to the manufacturer's instructions. Control siRNA- and Rab21 siRNA/EEA1 siRNA-treated cells ($0.75–1 \times 10^6$ cells each) were injected in a 1:1 ratio into the tail vein of 15 mice and lungs were collected 48 h after injection. This animal number has previously been sufficient for statistical significance in a similar experimental set-up[48,49]. The left lung of each mouse was formalin fixed and processed for frozen sections to be analysed by fluorescence microscopy and right lungs were processed into a cell suspension by collagenase I treatment as described in refs 48,49 and the number of fluorescently labelled cells was analysed by flow cytometry using LSRFortessa from BD Biosciences. The analyses were blinded such that the investigator analysing the data was unaware of the identity of the labelled cell populations. The quantification shows the ratio of Ctrl siRNA- and Rab21 siRNA- or EEA1 siRNA-treated cells in each lung. No blinding or randomization was performed as both cell types are co-injected in the same recipient animals simultaneously and analysed from the same samples using flow cytometry.

Mass spectrometry. Protein samples obtained from subcellular fractionation of WT MEFs were separated by SDS–PAGE and allowed to migrate 20 mm into a 4–12% polyacrylamide gel. Following staining with InstantBlue (Expedeon), gel lanes were sliced into ten 2-mm bands and subjected to in-gel digestion with trypsin as described previously[50] with modifications. Tryptic peptides were evaporated to dryness, dissolved in 1% HCOOH and 5 µl was submitted to LC–MS/MS analysis. The LC–MS/MS analysis was performed on a nanoflow HPLC system (EasyNano, Thermo Fisher Scientific) coupled to the LTQ Orbitrap Velos Pro mass spectrometer (Thermo Fisher Scientific) equipped with a nanoelectrospray ionization source. Peptides were first loaded on a trapping column and subsequently separated inline on a 15 cm C_{18} column (75 µm × 15 cm, Magic 5 µm 200 Å C_{18}, Michrom BioResources). The mobile phase consisted of water/acetonitrile (98:2 (v/v)) with 0.2% formic acid (solvent A) or acetonitrile/water (95:5 (v/v)) with 0.2% formic acid (solvent B). A linear 50 min gradient from 5% to 35% B was used to elute peptides.

MS data were acquired automatically using Thermo Xcalibur software (Thermo Fisher Scientific). An information-dependent acquisition method consisted of a TOF MS survey scan of mass range 300–2,000 m/z. The data files were searched for protein identification using Proteome Discoverer (1.4) connected to in-house Mascot (v. 2.4) software. Data were searched against the SwissProt database (release 2014_08). Carbamidomethylation of cysteine was set as a fixed modification and oxidation of methionine was allowed as a variable modification. Only tryptic peptides were considered, with up to one missed cleavage permitted. Monoisotopic precursor mass values were used, and only doubly and triply charged precursor ions were considered. Data were validated in Scaffold (version 3.6) using a threshold of identification of at least 50% probability at the peptide level, at least 99% probability at the protein level and assignment of at least two unique, validated peptides. These acceptance criteria resulted in an estimated protein false discovery rate of 0.1% for all data sets.

Data were converted using PRIDE Converter 2 (ref. 51), validated using PRIDE Inspector (version 2.5; ref. 52). Details of all identified proteins are provided in Supplementary Table 1.

Proteins identified in the various cellular fractions and described to be components of the Geiger Adhesome[29] were hierarchically clustered on the basis of uncentred Pearson correlation using Cluster 3.0 (C Clustering Library, version 1.50; ref. 53) and visualized using Java TreeView (version 1.1.6r2; ref. 54). Protein–protein interaction (PPI) network analysis was performed using Cytoscape (version 3.2; ref. 55). Proteins were mapped onto a merged human interactome consisting of PPIs reported in the Protein Interaction Network Analysis platform *Homo sapiens* network (May 2014)[56]. Identified proteins were also compared to the proteins identified in various published data set of isolated adhesion complexes[57–61].

Accession numbers. The proteomic data are deposited in the PRIDE database (http://www.ebi.ac.uk/pride)[62] under project accession no. PXD001870 and project http://dx.doi.org/10.6019/PXD001870.

Statistics. The data sets with sufficient n numbers to run the D'Agnostino & Pearson Omnibus were all found to be normally distributed; therefore, these data were analysed using unpaired Student's t-test. For data sets where the n numbers were too small for the D'Agnostino and Pearson Omnibus normality test, we assumed normal distribution based on the appearance of the data. Statistical significance was analysed using Student's t-test with normal distribution and equal variance. $P < 0.05 = ^{*}$, $P < 0.01 = ^{**}$, $P < 0.005 = ^{***}$. No statistical method was used to predetermine sample size.

40. Wennerberg, K. *et al.* The cytoplasmic tyrosines of integrin subunit β1 are involved in focal adhesion kinase activation. *Mol. Cell. Biol.* **20,** 5758–5765 (2000).
41. Schlaepfer, D. D. *et al.* Tumor necrosis factor-α stimulates focal adhesion kinase activity required for mitogen-activated kinase-associated interleukin 6 expression. *J. Biol. Chem.* **282,** 17450–17459 (2007).
42. Altschuler, Y. *et al.* Redundant and distinct functions for dynamin-1 and dynamin-2 isoforms. *J. Cell Biol.* **143,** 1871–1881 (1998).
43. Lawe, D. C., Patki, V., Heller-Harrison, R., Lambright, D. & Corvera, S. The FYVE domain of early endosome antigen 1 is required for both phosphatidylinositol 3-phosphate and Rab5 binding. Critical role of this dual interaction for endosomal localization. *J. Biol. Chem.* **275,** 3699–3705 (2000).
44. Miyauchi, K., Kim, Y., Latinovic, O., Morozov, V. & Melikyan, G. B. HIV enters cells via endocytosis and dynamin-dependent fusion with endosomes. *Cell* **137,** 433–444 (2009).
45. Macia, E. *et al.* Dynasore, a cell-permeable inhibitor of dynamin. *Dev. Cell.* **10,** 839–850 (2006).
46. Virtakoivu, R., Pellinen, T., Rantala, J. K., Perala, M. & Ivaska, J. Distinct roles of AKT isoforms in regulating β1-integrin activity, migration, and invasion in prostate cancer. *Mol. Biol. Cell* **23,** 3357–3369 (2012).
47. Azioune, A., Storch, M., Bornens, M., Thery, M. & Piel, M. Simple and rapid process for single cell micro-patterning. *Lab Chip* **9,** 1640–1642 (2009).
48. Arjonen, A. *et al.* Mutant p53-associated myosin-X upregulation promotes breast cancer invasion and metastasis. *J. Clin. Invest.* **124,** 1069–1082 (2014).
49. Vuoriluoto, K. *et al.* Vimentin regulates EMT induction by Slug and oncogenic H-Ras and migration by governing Axl expression in breast cancer. *Oncogene* **30,** 1436–1448 (2011).
50. Shevchenko, A. *et al.* A strategy for identifying gel-separated proteins in sequence databases by MS alone. *Biochem. Soc. Trans.* **24,** 893–896 (1996).
51. Cote, R. G. *et al.* The PRIDE Converter 2 framework: an improved suite of tools to facilitate data submission to the PRIDE database and the ProteomeXchange consortium. *Mol. Cell Proteomics* **12,** 1682–1689 (2012).
52. Wang, R. *et al.* PRIDE Inspector: a tool to visualize and validate MS proteomics data. *Nat. Biotech.* **30,** 135–137 (2012).
53. Hoon, M. J. L. d., Imoto, S., Nolan, J. & Miyano, S. Open source clustering software. *Bioinformatics* **20,** 1453–1454 (2004).
54. Saldanha, A. J. Java Treeview—extensible visualization of microarray data. *Bioinformatics* **20,** 3246–3248 (2004).
55. Saito, R. *et al.* A travel guide to Cytoscape plugins. *Nat. Methods* **9,** 1069–1076 (2012).
56. Cowley, M. J. *et al.* PINA v2.0: mining interactome modules. *Nucleic Acids Res.* **40,** D862–D865 (2012).
57. Schiller, H. B., Friedel, C. C., Boulegue, C. & Fässler, R. Quantitative proteomics of the integrin adhesome show a myosin II-dependent recruitment of LIM domain proteins. *EMBO Rep.* **12,** 259–266 (2011).
58. Schiller, H. B. *et al.* β1- and αv-class integrins cooperate to regulate myosin II during rigidity sensing of fibronectin-based microenvironments. *Nat. Cell Biol.* **15,** 625–636 (2013).

59. Humphries, J. D. *et al.* Proteomic analysis of integrin-associated complexes identifies RCC2 as a dual regulator of Rac1 and Arf6. *Sci. Signal.* **2,** ra51 (2009).
60. Ng, D. H. J., Humphries, J. D., Byron, A., Millon-Frémillon, A. & Humphries, M. J. Microtubule-dependent modulation of adhesion complex composition. *PLoS ONE* **9,** e115213 (2014).
61. Robertson, J. *et al.* Defining the phospho-adhesome through the phosphoproteomic analysis of integrin signalling. *Nat. Commun.* **6,** 6265 (2015).
62. Vizcaino, J. A. *et al.* The Proteomics Identifications (PRIDE) database and associated tools: status in 2013. **41,** D1063–D1069 (2013).

DOI: 10.1038/ncb3250

nature cell biology

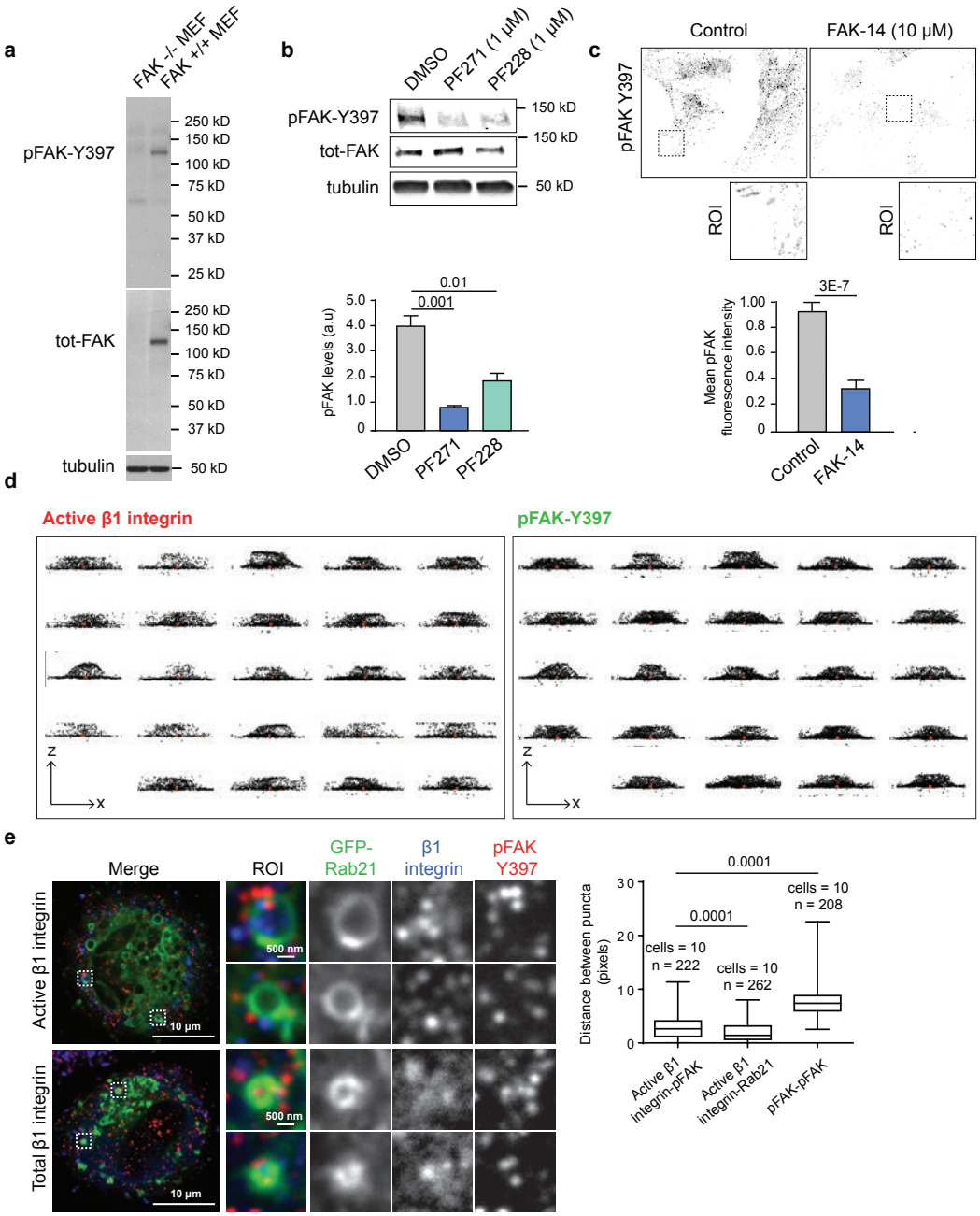

Supplementary Figure 1 Validation of the pFAK-Y397 antibody. **a, b** Validation of the pFAK-Y397 antibody in FAK-/- and FAK+/+ MEF cell lysates (**a**) and in TIFFs in the presence of FAK-Y397 phosphorylation inhibitors (1 μM PF271 or PF228) (**b**) (mean ± SEM, n = 3 independent experiments). Statistics source data can be found in Supplementary Table 2. **c,** Quantification of pFAK-Y397 levels following FAK-14 inhibitor (10 μM) treatment. Representative confocal images and ROIs of focal adhesions are shown (mean fluorescence intensity ± SEM, n = 22 cells pooled from two independent experiments). **d,** Individual fluorescence density plots of MDA-MB-231 cells plated on crossbow-shaped fibronectin-coated micropatterns and stained for active β1-integrin and pFAK-Y397. Shown are x-axis views. The analysis of these cells was used to generate the 3D probabilistic density plots shown in Figure 1a. **e**, Confocal images of pFAK-Y397 and total or active β1-integrin staining in GFP-Rab21 overexpressing TIFFs plated on fibronectin (45 min). Representative ROIs from endosomes and box plot of the distance between adjacent puncta of active β1-integrin and pFAK or Rab21 in GFP-Rab21-positive endosomes or of pFAK and pFAK outside the endosomes (in pixels) (box plots show the 25th–75th percentiles delineated by the upper and lower limits of the box; the median is shown by the horizontal line inside the box. Whiskers indicate maxima and minima). n= the number of active β1-integrin-pFAK, active β1-integrin-Rab21 and pFAK-pFAK doublets (indicated in the figure) analysed from multiple cells (numbers indicated in the figure) from three independent experiments are indicated. Mann-Whitney test *P* values are provided.

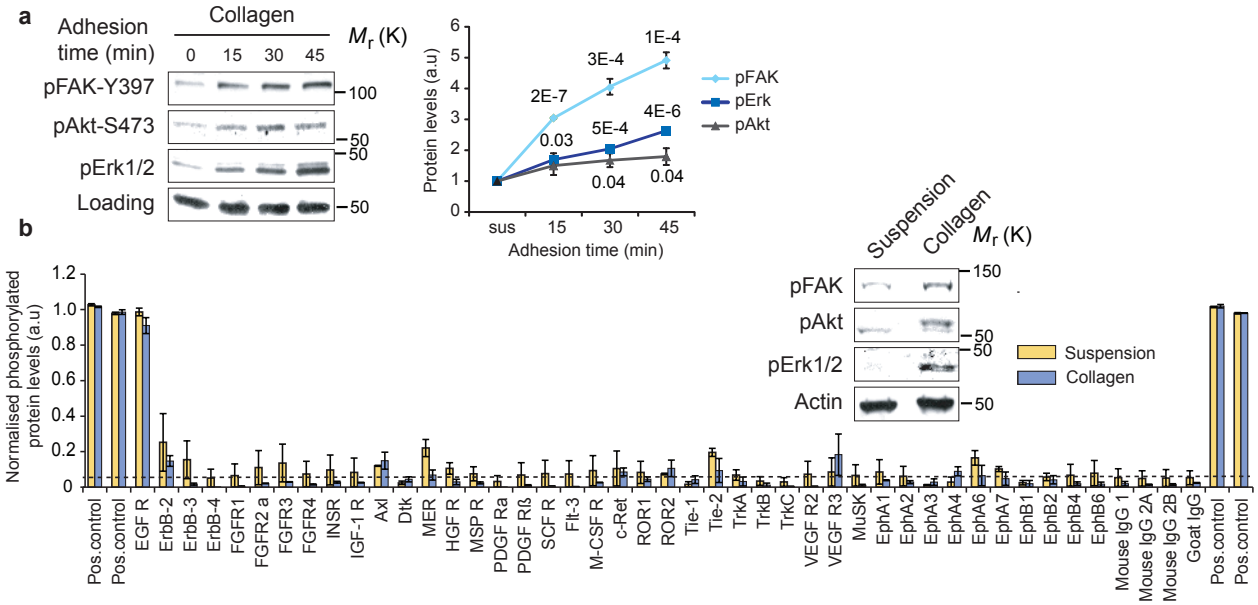

Supplementary Figure 2 ECM-induced downstream signalling is not due to growth factor receptor activation. **a**, Quantification of kinase activity in NCI-H460 cells plated on collagen. Representative blots are shown (mean ± SEM, n= 3 independent experiments). **b**, Quantification of human phospho-receptor tyrosine kinase array in NCI-H460 cells kept in suspension or plated on collagen (45 min). Positive control is an antibody against phospho-tyrosine. Representative blots of cell lysates used for the array are shown (mean phosphoprotein detection ± SEM from two independent experiments). Student's two-tailed unpaired t-test *P* values are provided and statistics source data can be found in Supplementary Table 2. Uncropped images of blots are shown in supplementary figure 9.

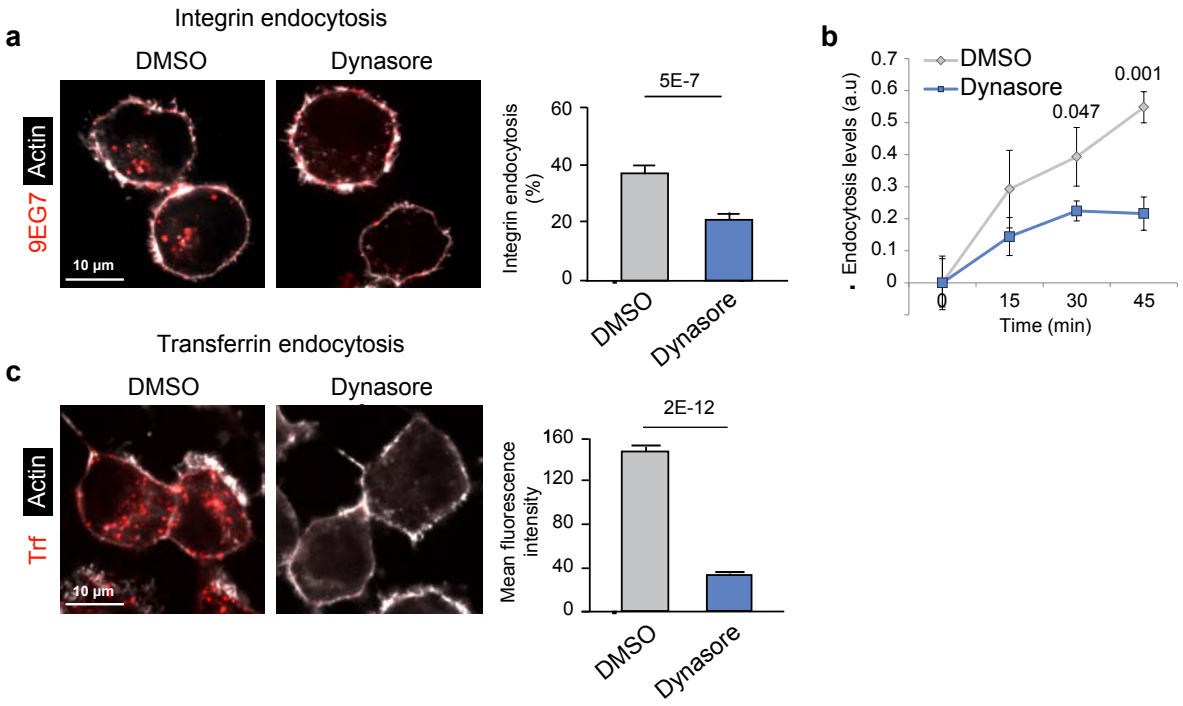

Supplementary Figure 3 Dynamin inhibition downregulates integrin receptor endocytosis. **a, b** Integrin receptor endocytosis in NCI-H460 cells plated on collagen for 45 min in the presence of active β1-integrin (9EG7) antibody (45 min) ± dynasore. **a,** Representative confocal images and quantification of the proportion of endocytosed integrin receptors based on antibody staining (n(DMSO)=52 cells, n(dynasore)=54 cells, pooled from three independent experiments, mean ± SEM). **b,** Flow cytometry-based analysis of integrin endocytosis. Receptor internalisation, at the indicated time points, was calculated as an inverse ratio of total 9EG7-labelled integrin remaining on the cell surface compared to time point 0 (mean ± SEM, n=3 independent experiments). **c,** Transferrin endocytosis in NCI-H460 cells plated on collagen for 45 min in the presence of 555-labelled-transferrin (15 min) ± dynasore. Representative confocal images and quantification of the total levels of endocytosed transferrin are shown (n(DMSO)=35 cells, n(dynasore)=32 cells, pooled from three independent experiments, mean ± SEM). Student's two-tailed unpaired t-test *P* values are provided. Statistics source data can be found in Supplementary Table 2.

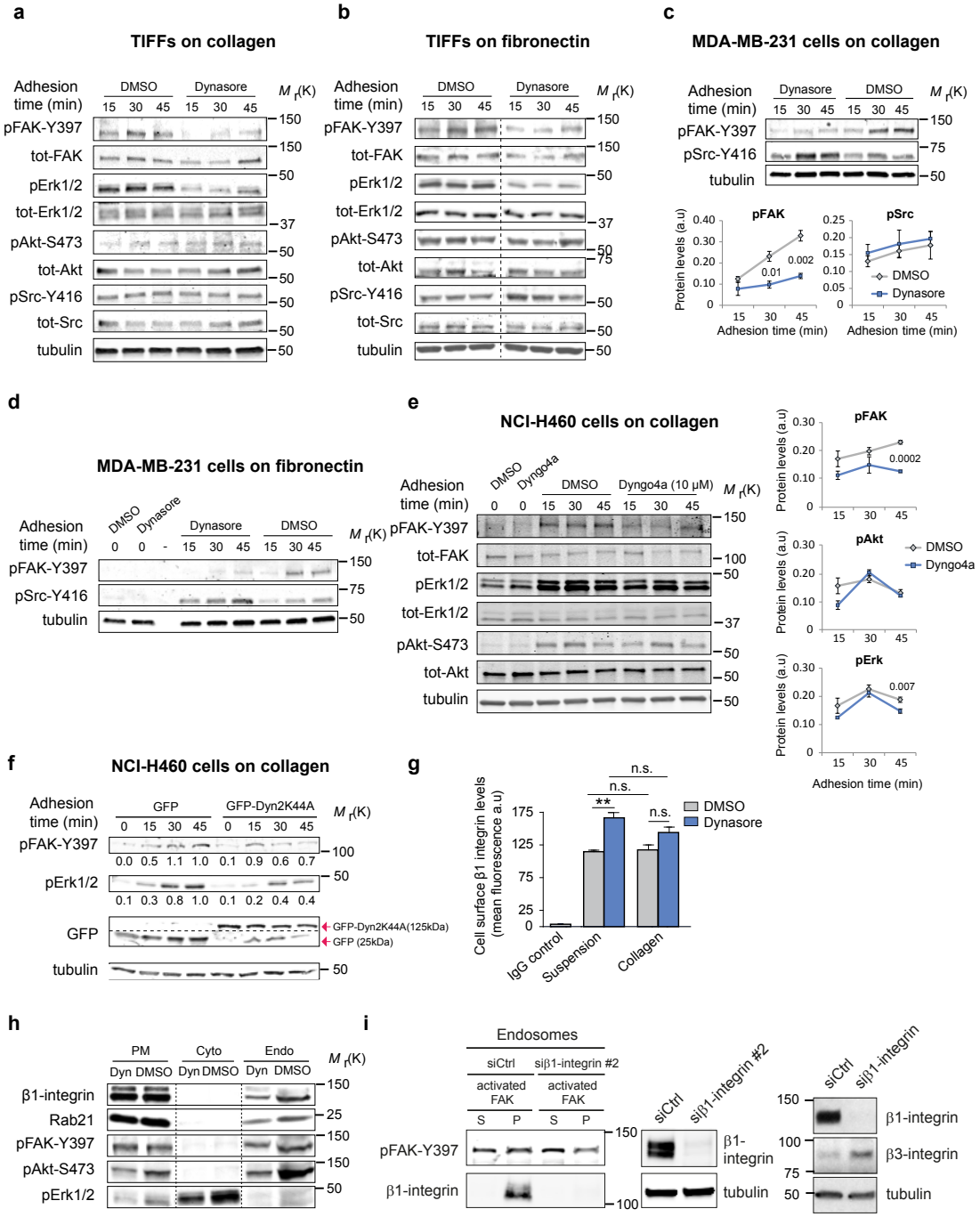

Supplementary Figure 4 Inhibition of integrin endocytosis attenuates integrin signalling. **a, b** Representative blots of kinase activity in TIFFs plated on collagen (**a,** quantified in Fig. 3c) and fibronectin (**b,** quantified in Fig. 3d) ± dynasore. **c, d,** Analysis of kinase activity in MDA-MB-231 cells plated on collagen (**c**) and fibronectin (**d**) ± dynasore. Representative blots (**c, d**) and quantification (**c**) are shown (mean ± SEM, n=3 independent experiments). **e**, Analysis of kinase activity in NCI-H460 cells plated on collagen ± 10 µM Dyngo4a. Representative blots and quantifications are shown (mean ± SEM, n=3 independent experiments). **f**, Analysis of kinase activity in GFP or GFP-Dyn2K44A overexpressing NCI-H460 cells plated on collagen. Representative blot and quantification of normalised band integrated densities are shown (three independent experiments). **g**, Flow cytometry quantification of total cell surface β1-integrin levels in NCI-H460 cells held in suspension or plated on collagen (45 min) ± dynasore (mean fluorescence ± SEM, n=3 independent experiments). **h**, Subcellular fractionation of NCI-H460 cells plated on collagen (45 min) ± dynasore. Representative blots of the plasma membrane (PM), cytoplasm (Cyto) and endosomal fractions (Endo) are shown (three independent experiments). **i,** Representative immunoblot analysing the recruitment of recombinant FAK to purified endosomes derived from either control- or β1-integrin-silenced FAK -/- MEFs (different siRNA to one used in Fig. 4c; three independent experiments). Please note that silencing of β1-integrin induces cellular levels of β3-integrin. This might contribute to the residual FAK recruitment to the β1-integrin silenced endosomal fraction. Student's two-tailed unpaired t-test *P* values are provided. Statistics source data can be found in Supplementary Table 2. Uncropped images of blots are shown in supplementary figure 9.

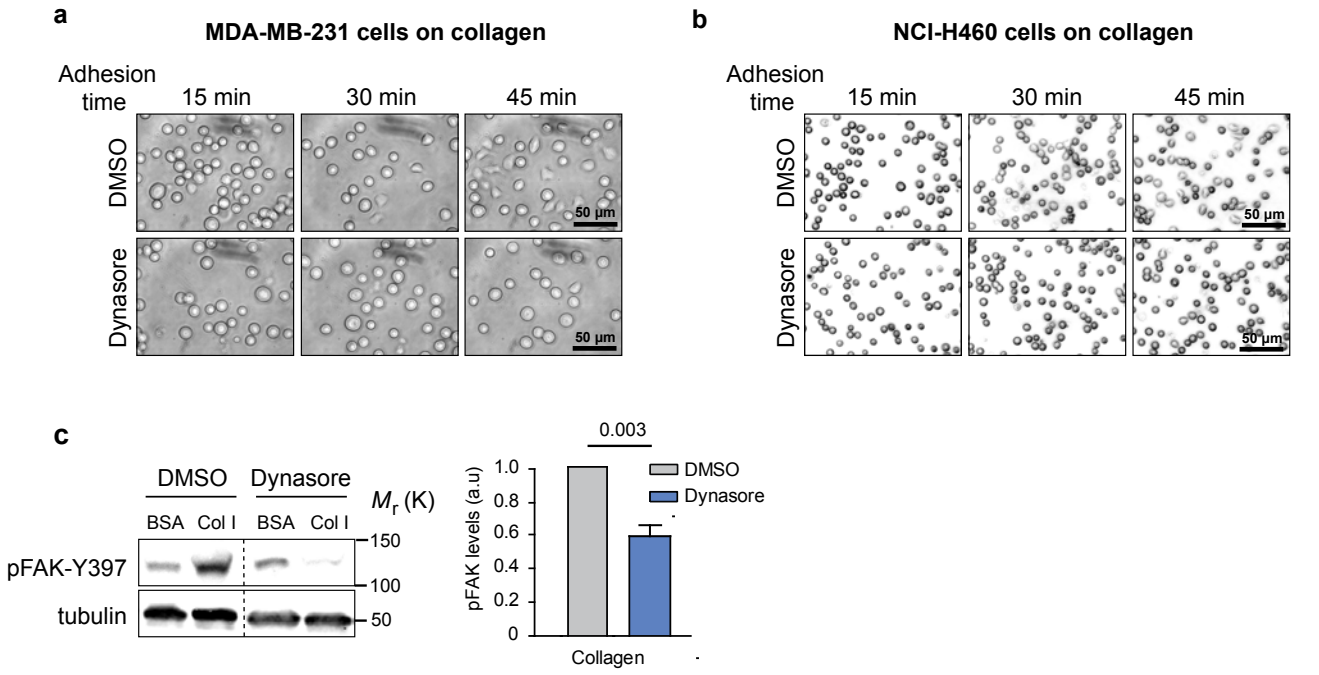

Supplementary Figure 5 Dynamin inhibition affects cell spreading. MDA-MB-231 cells (**a**) or NCI-H460 cells (**b**) plated on collagen for the indicated times ± dynasore (three independent experiments). (**c**) Quantification of FAK activation (pFAK-Y397 levels) in NCI-H460 cells incubated with collagen (Col I) or BSA-coated beads in suspension (45 min) ± dynasore (mean ± SEM, n=3 independent experiments). Student's two-tailed unpaired t-test *P* values are provided and statistics source data can be found in Supplementary Table 2. Uncropped images of blots are shown in supplementary figure 9.

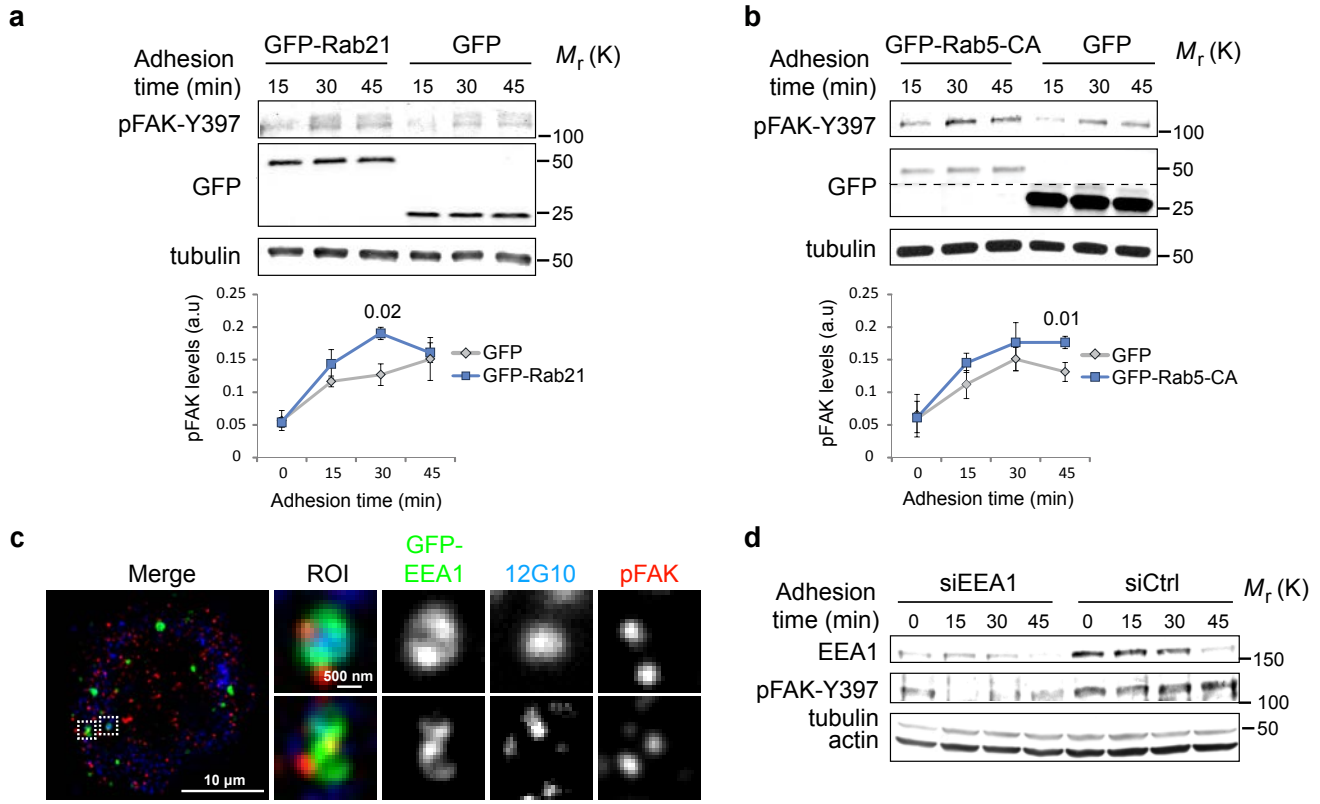

Supplementary Figure 6 Rab5, Rab21 and EEA1 are important for integrin-mediated FAK activation. **a, b,** Representative blots and quantification of pFAK levels in GFP and GFP-Rab21 (**a**) or GFP-Rab5-CA (**b**) overexpressing MDA-MB-231 cells plated on collagen (n(a)=3, n(b)=6 independent experiments, mean ± SEM). **c**, Active β1-integrin (12G10) and pFAK-Y397 localization in GFP-EEA1 expressing TIFFs plated on fibronectin (45 min). **d**, Representative blot of pFAK-Y397 levels in control or EEA1 smart pool silenced NCI-H460 cells plated on collagen. Student's two-tailed unpaired t-test *P* values are provided and statistics source data can be found in Supplementary Table 2. Uncropped images of blots are shown in supplementary figure 9.

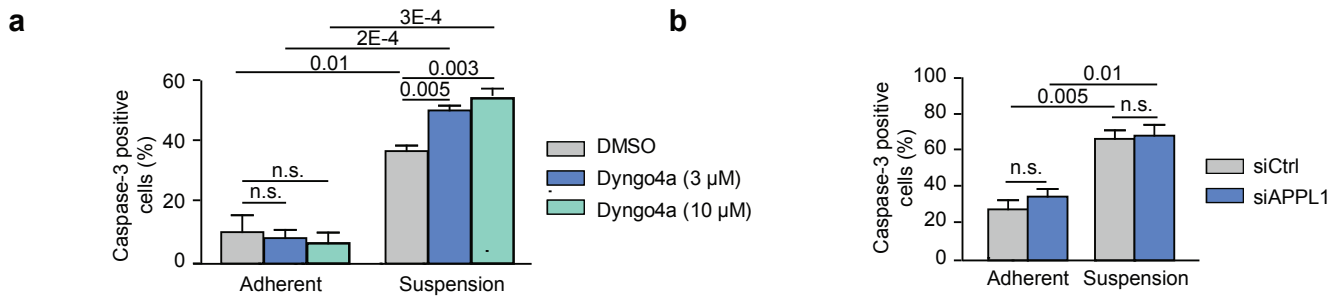

Supplementary Figure 7 APPL1 is not important for anoikis suppression. **a-b,** Quantification of caspase-3 positive apoptotic TIFFs ± Dyngo4a (**a**), and following APPL1 silencing (**b**) (mean fluorescence ± SEM, n=3 independent experiments). Student's t-test *P* values are provided and statistics source data can be found in Supplementary Table 2.

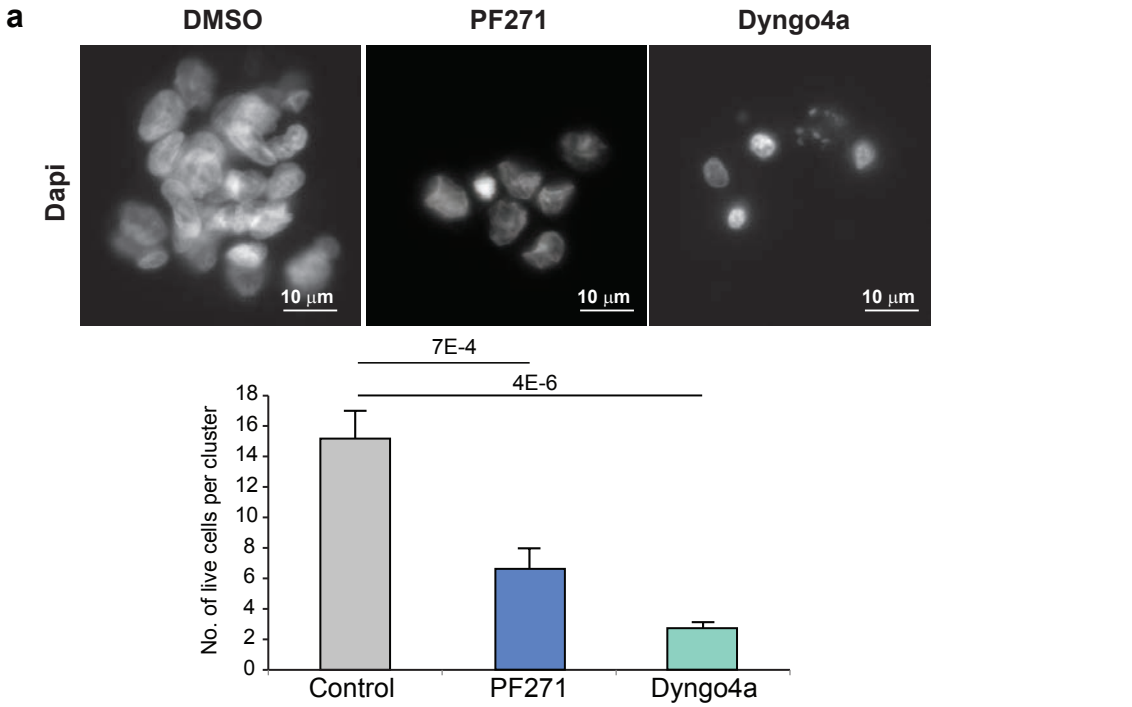

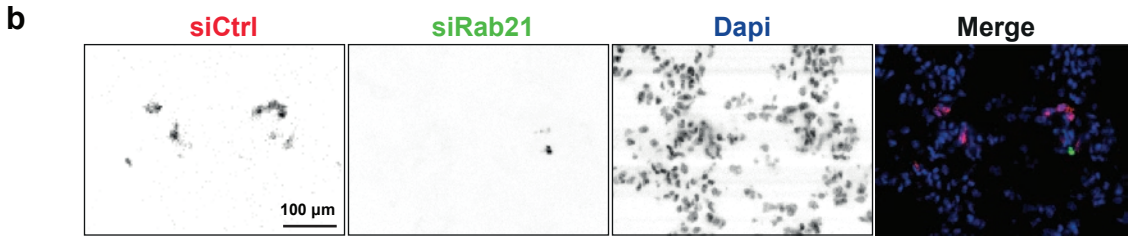

Supplementary Figure 8 Anchorage-independent growth and metastases of MDA-MB-231 cells are sensitive to FAK and dynamin inhibition and Rab21 silencing. **a,** MDA-MB-231 cells were plated on agar and incubated with the indicated drugs. Anchorage-independent growth was assessed by counting the number of cells per cluster with intact nuclei (mean ± SEM, n = 6 fields of view assessed from three independent experiments). **b,** Representative images showing extravasation of siCtrl- and siRab21-treated MDA-MB-231 cells in mouse lungs. Student's t-test *P* values are provided.

Figure 2.

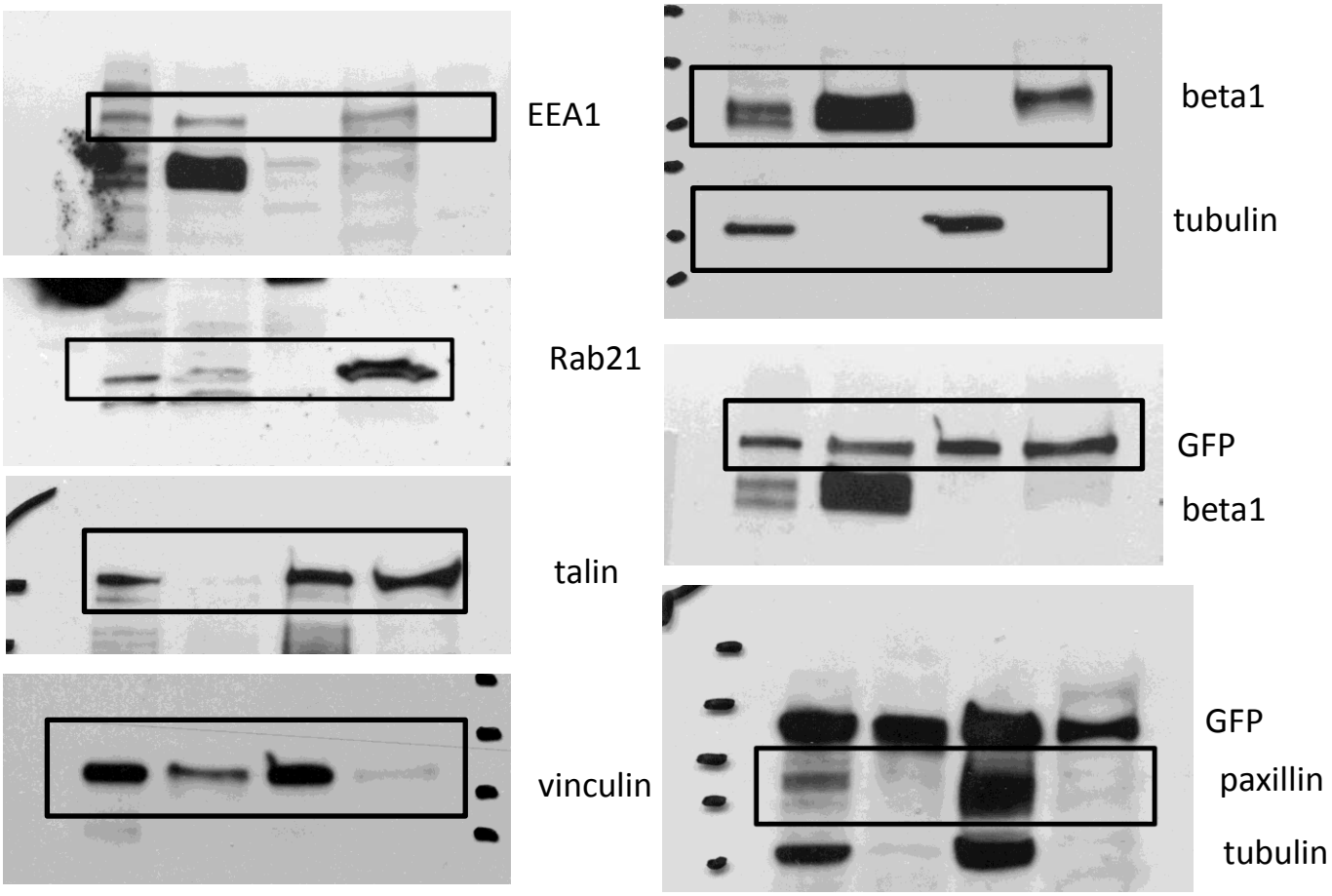

Supplementary Figure 9 Uncropped Western blots. Solid line boxes indicate the cropped areas shown in the figures. Dashed lines indicate the outlines of the filter for membranes processed with Odyssey where the background appears white and the signal is strong. In all the uncropped western blot images labelled with more than 1 proteins the filters have been simultaneously or sequentially blotted with the indicated specific antibodies.

Figure 3a.

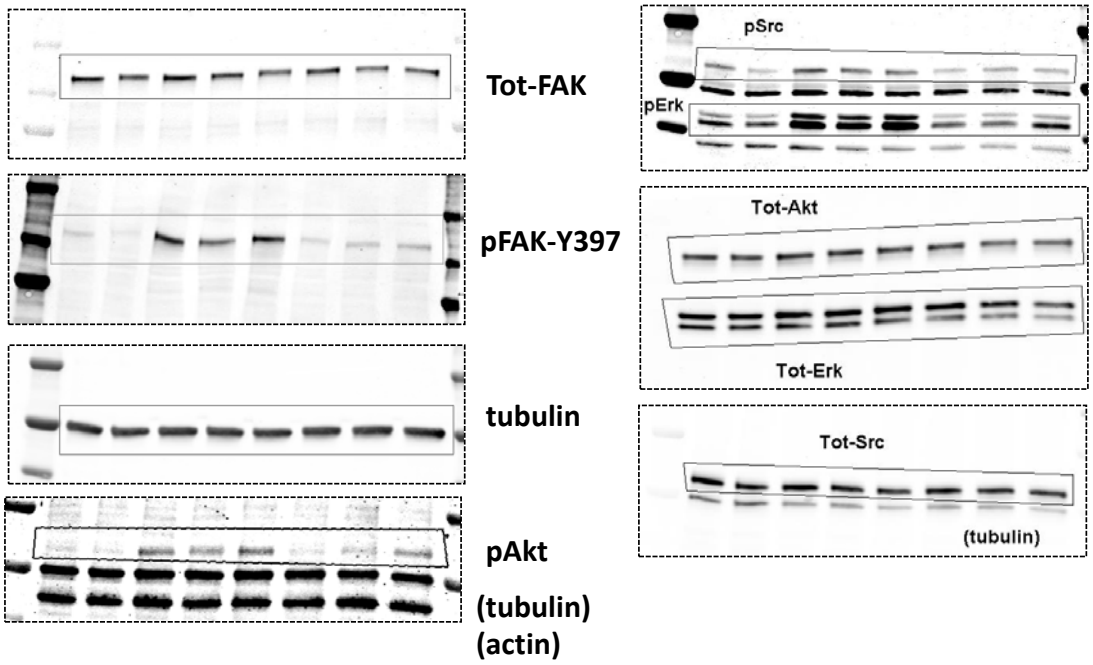

Figure 3b.

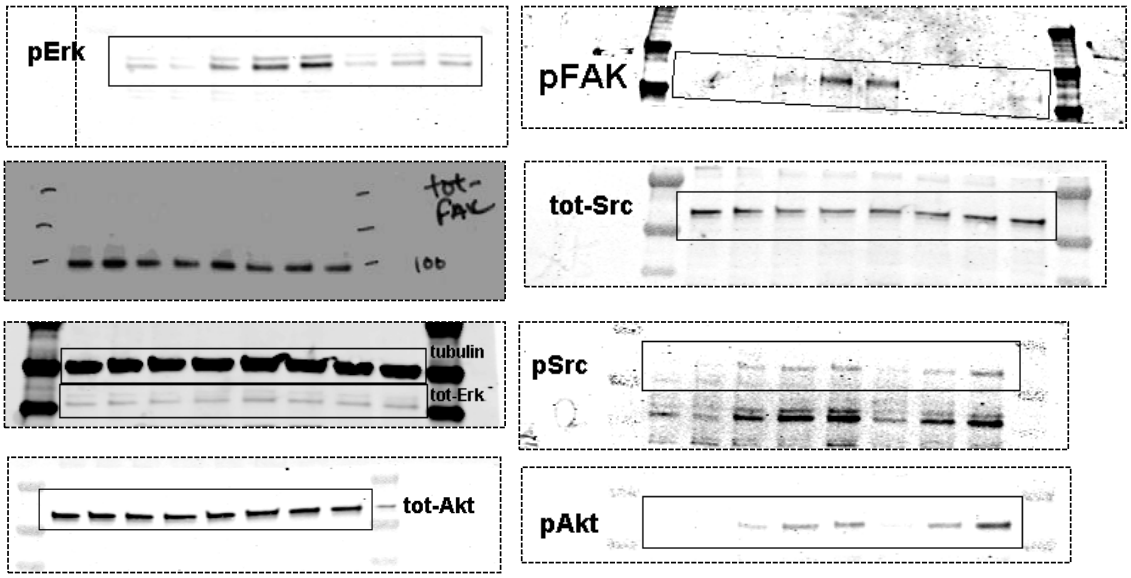

Supplementary Figure 9 continued

Figure 3f.

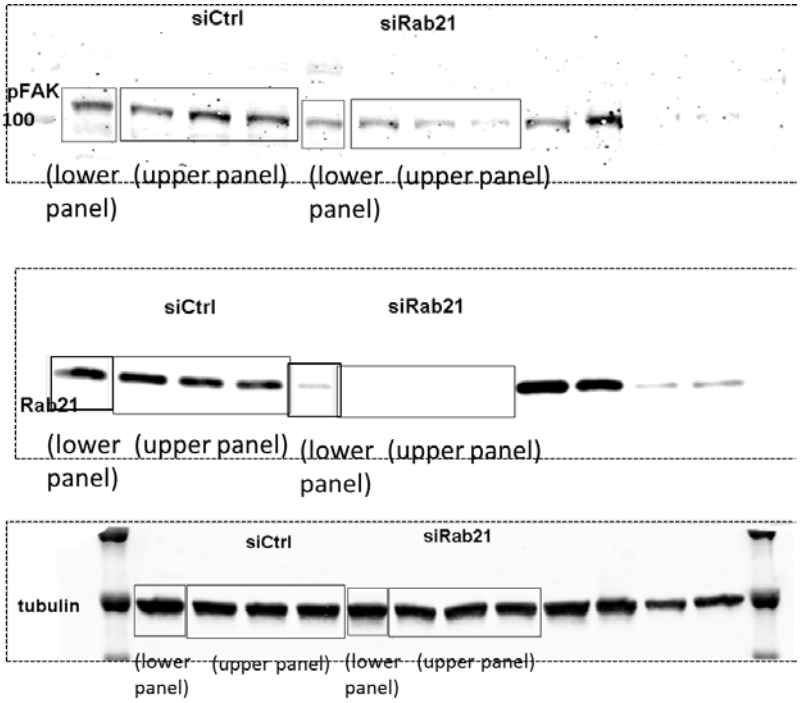

Figure 3g.

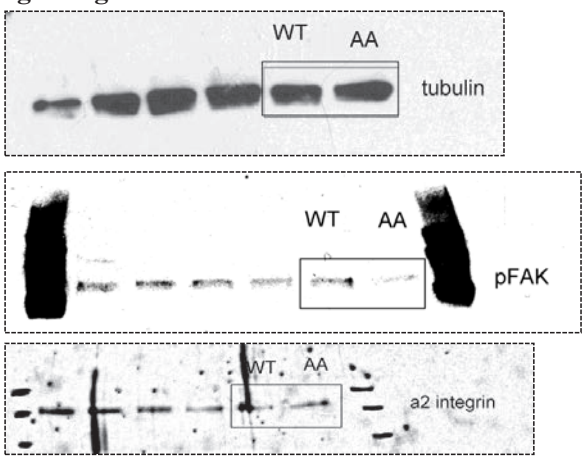

Supplementary Figure 9 continued

Figure 4a.

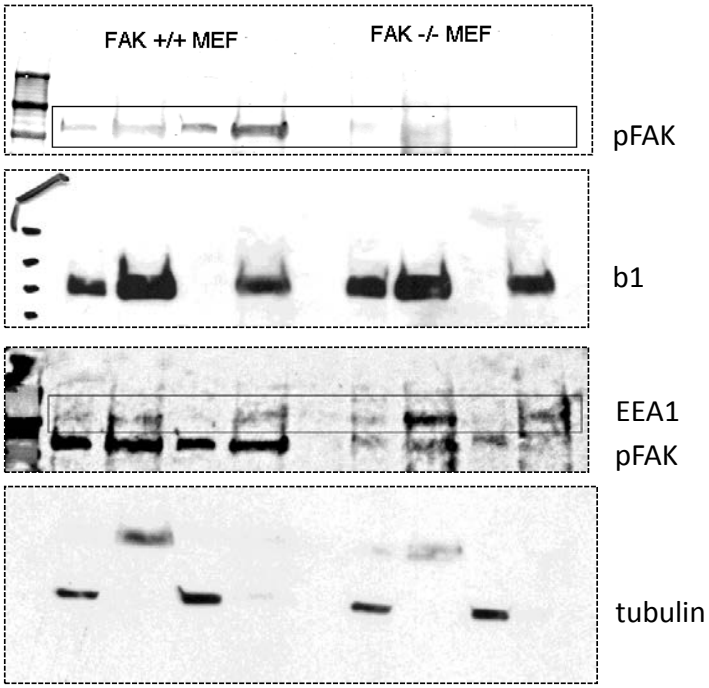

Figure 4b.

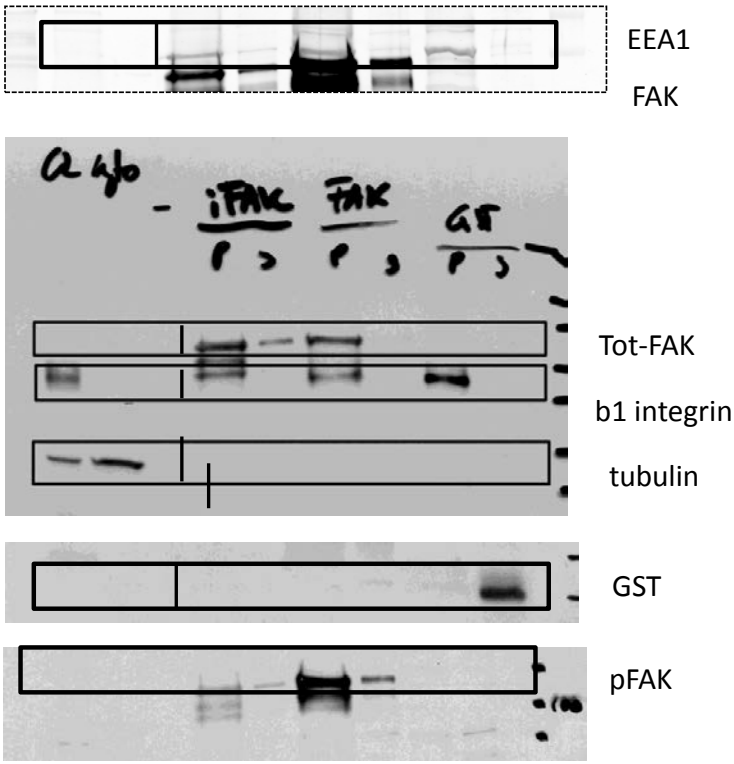

Supplementary Figure 9 continued

Figure 4c.

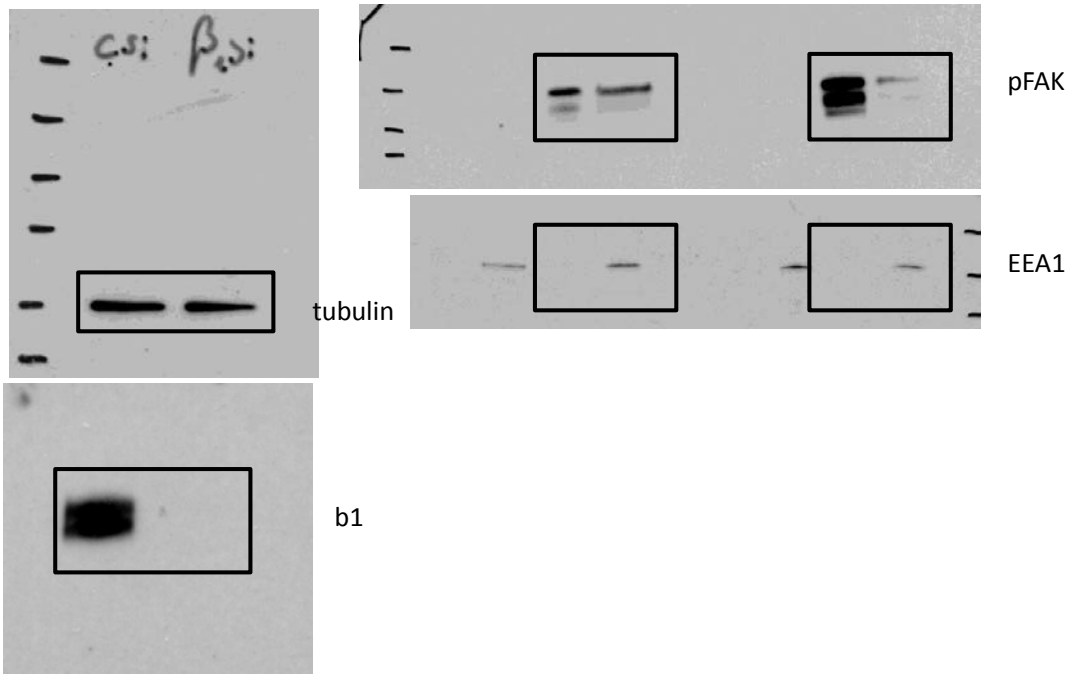

Figure 4d.

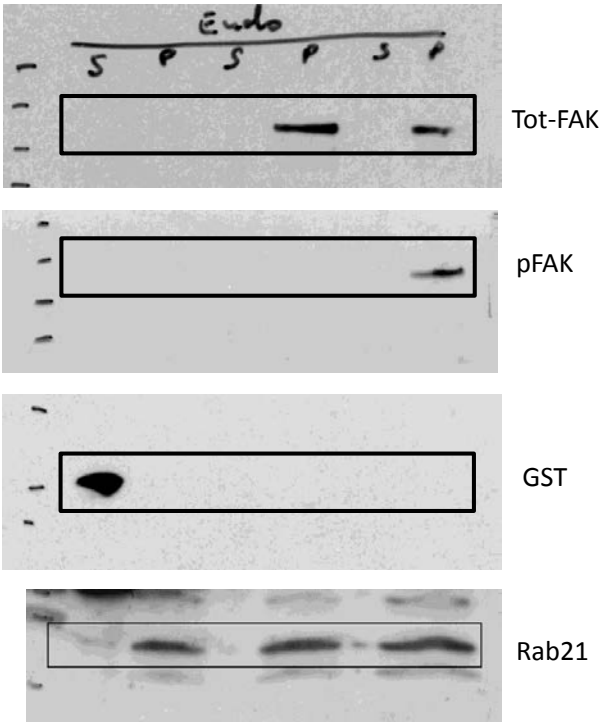

Supplementary Figure 9 continued

Figure 4e.

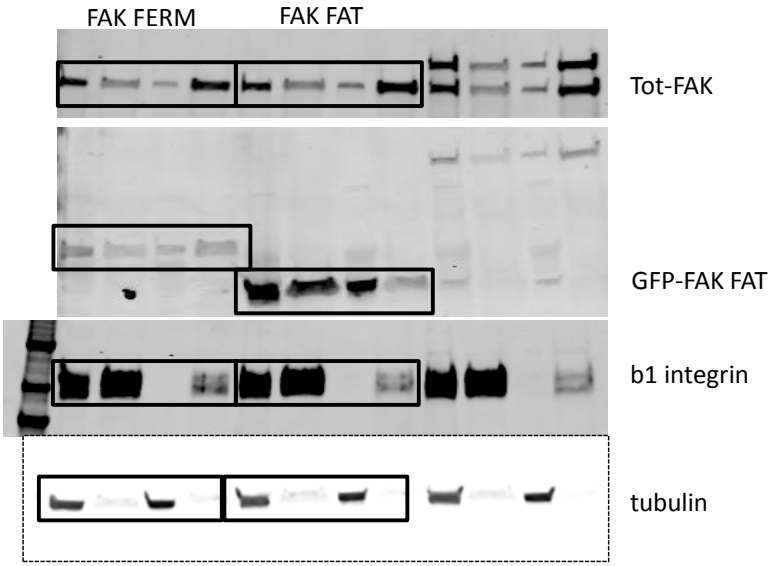

Figure 5a.

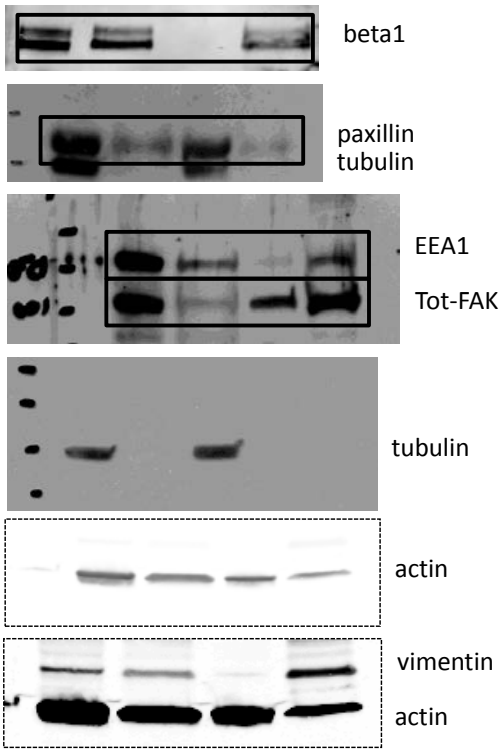

Supplementary Figure 9 continued

Figure 6a.

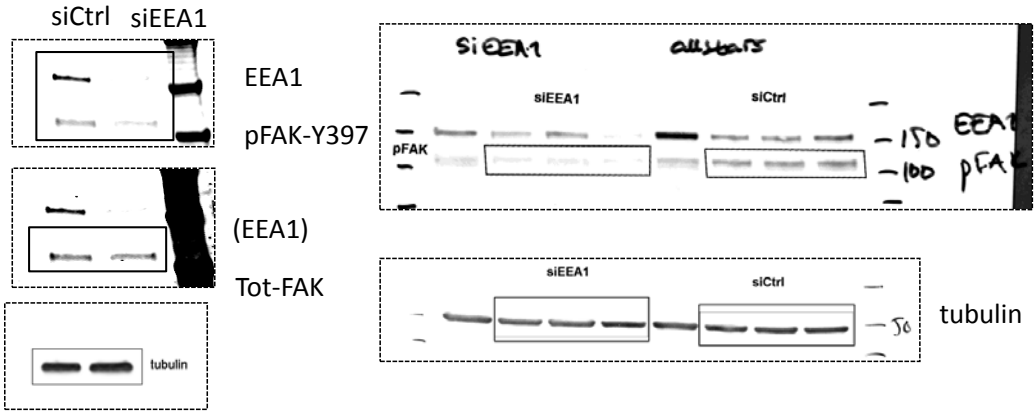

Figure 6b.

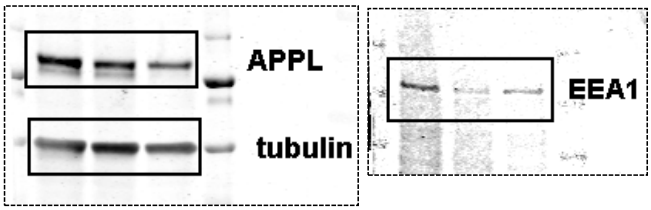

Figure 6c.

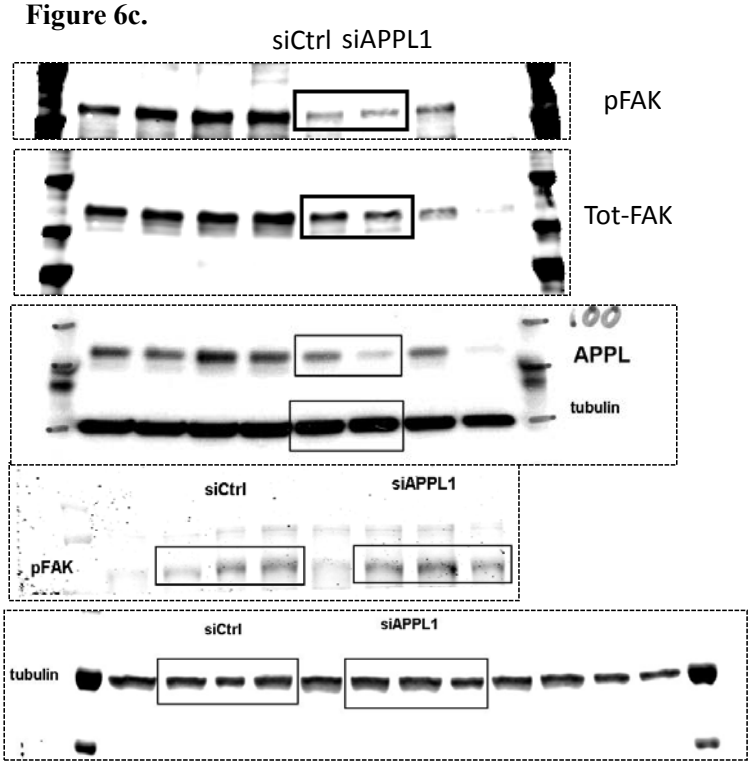

Supplementary Figure 9 continued

Figure 6d.

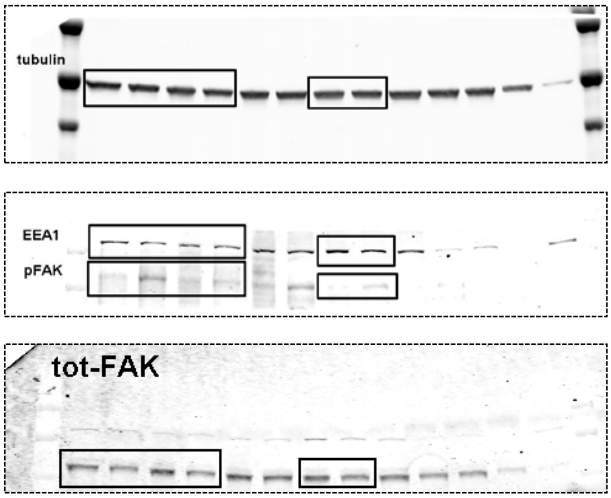

Figure 7b.

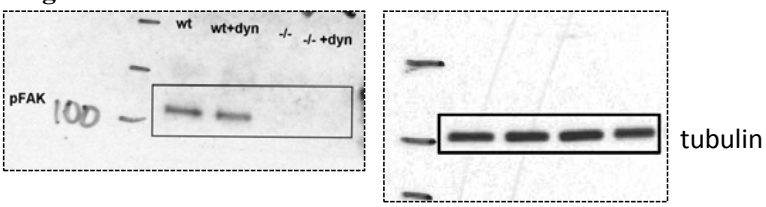

Figure 7f.

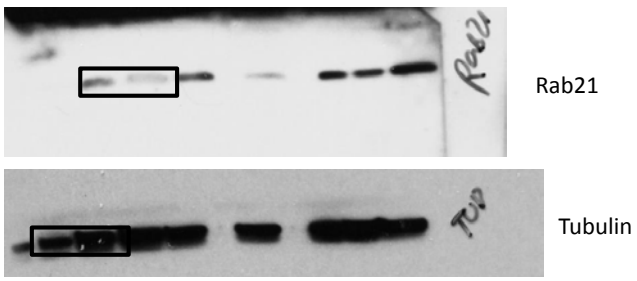

Figure 7g.

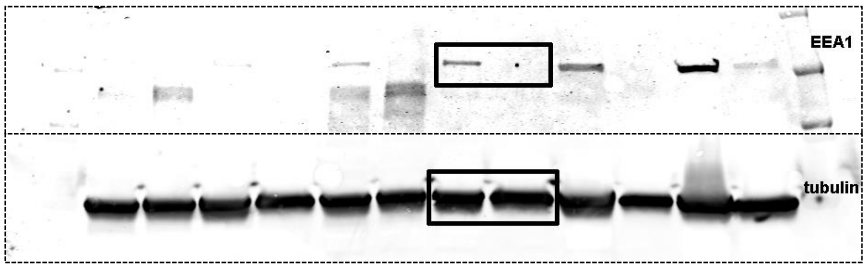

Supplementary Figure 9 continued

Supplementary Figure 1a.

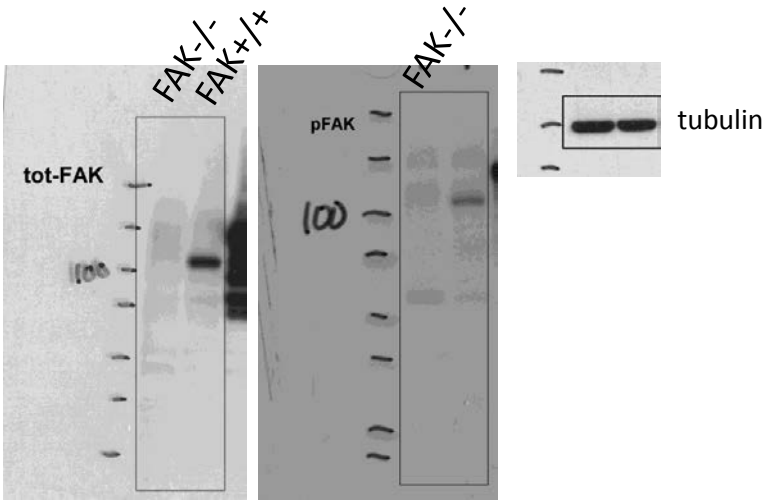

Supplementary Figure 1b.

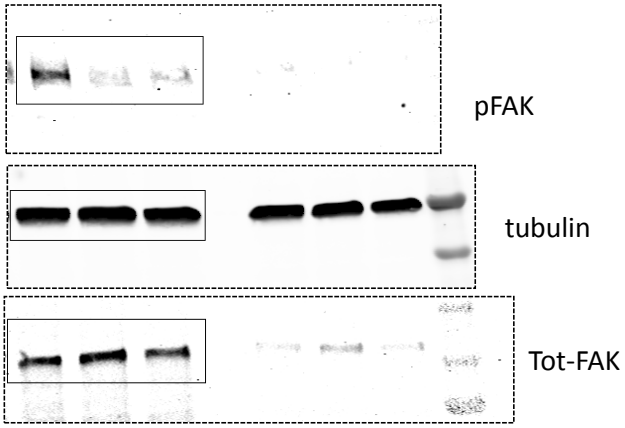

Supplementary Figure 2a.

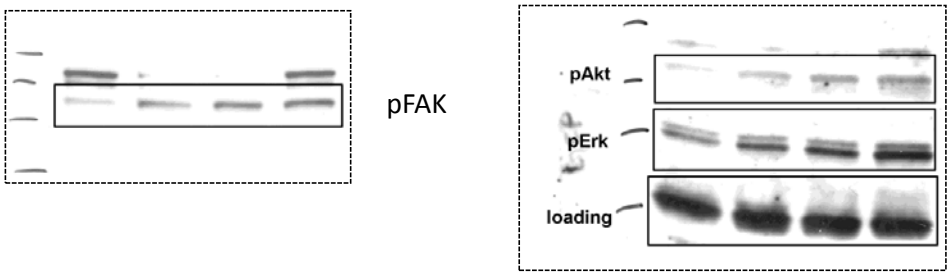

Supplementary Figure 9 continued

Supplementary Figure 2b.

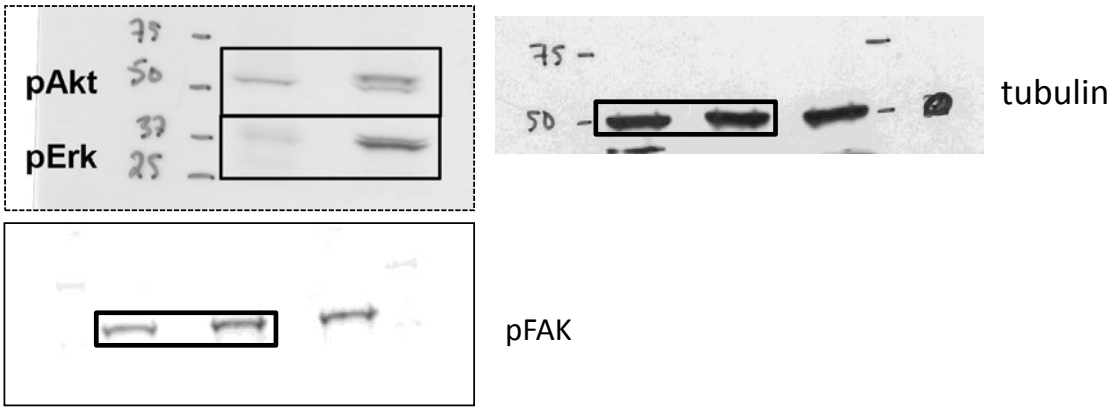

Supplementary Figure 4a.

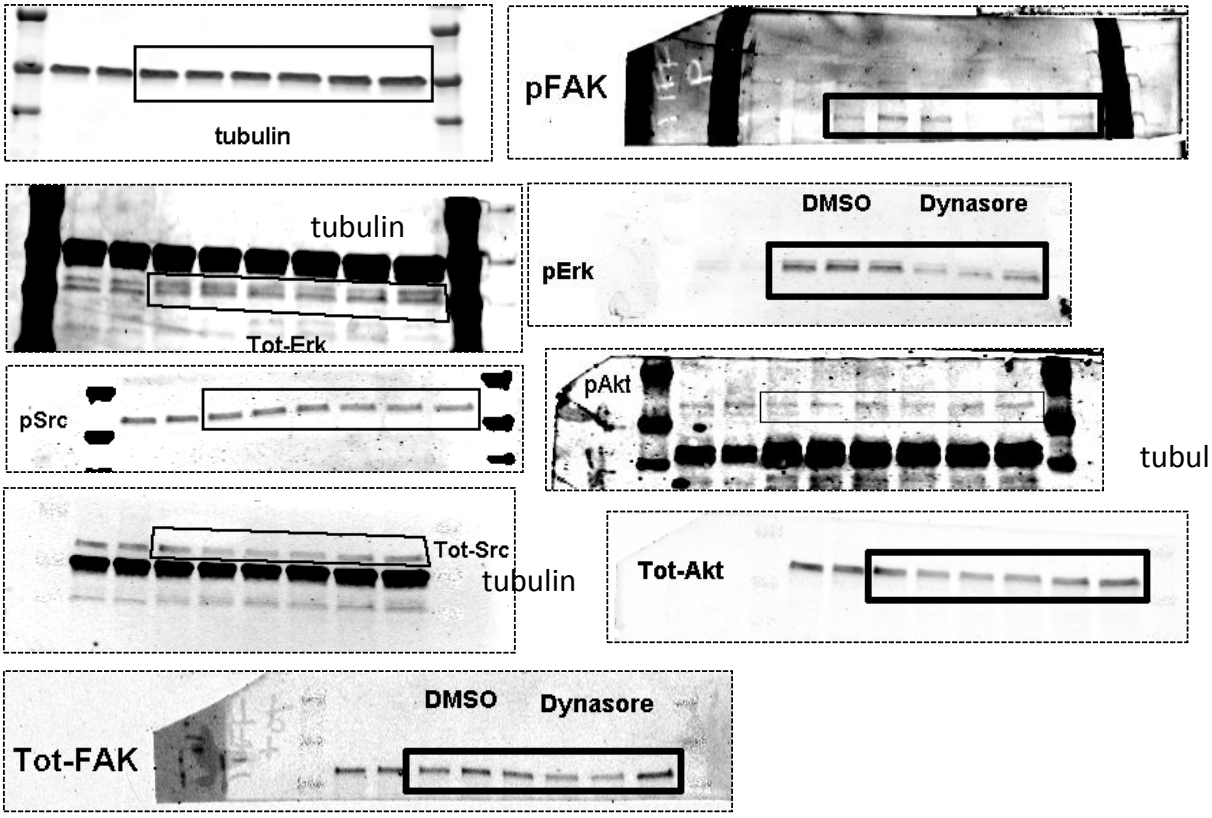

Supplementary Figure 9 continued

Supplementary Figure 4b.

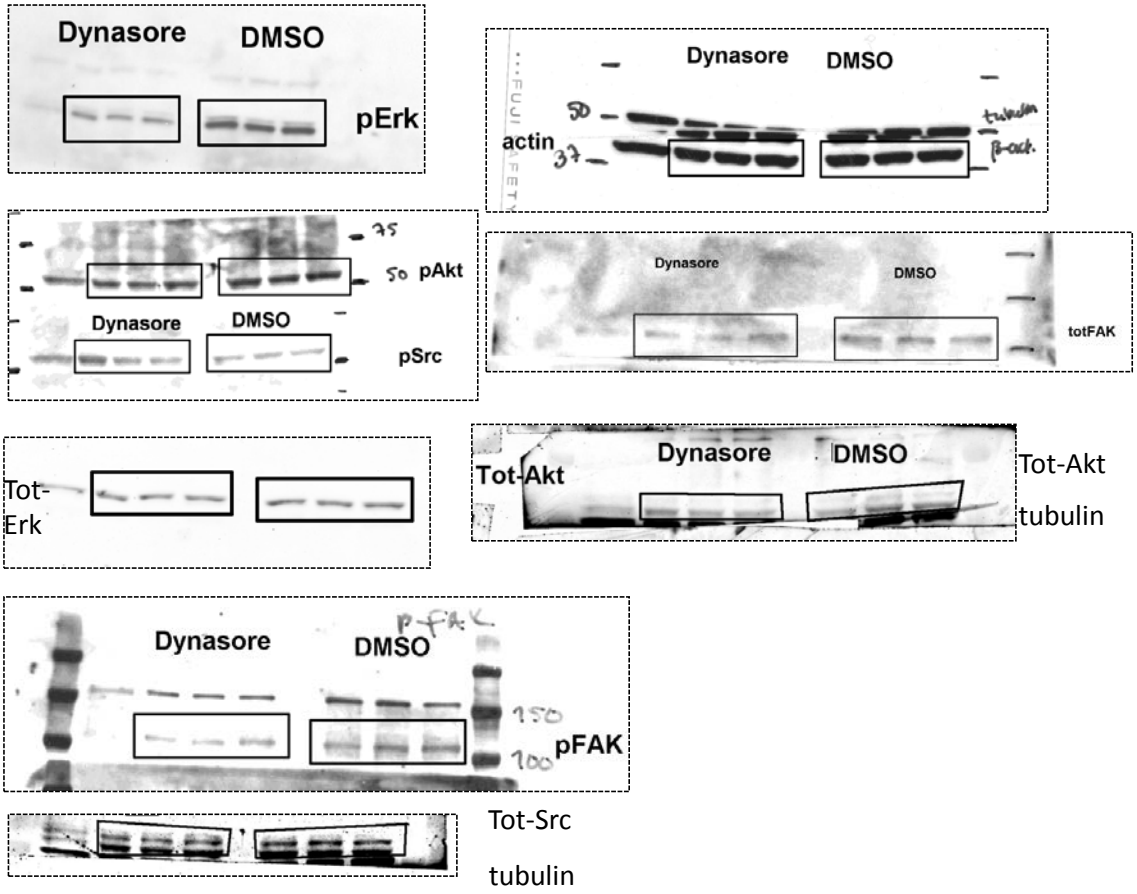

Supplementary Figure 4c.

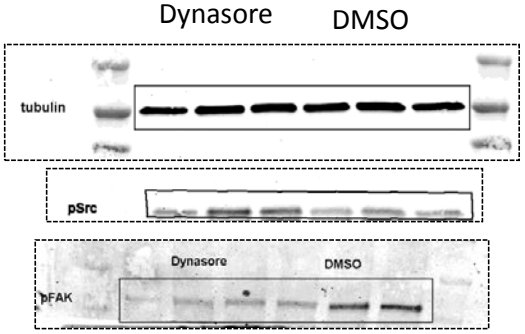

Supplementary Figure 4d.

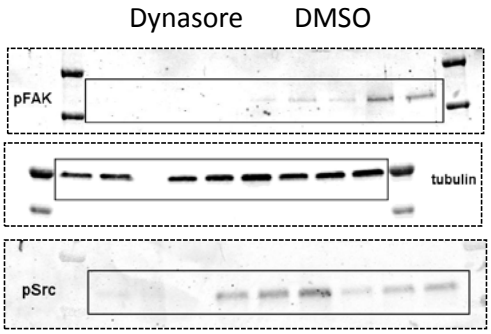

Supplementary Figure 9 continued

Supplementary Figure 4e.

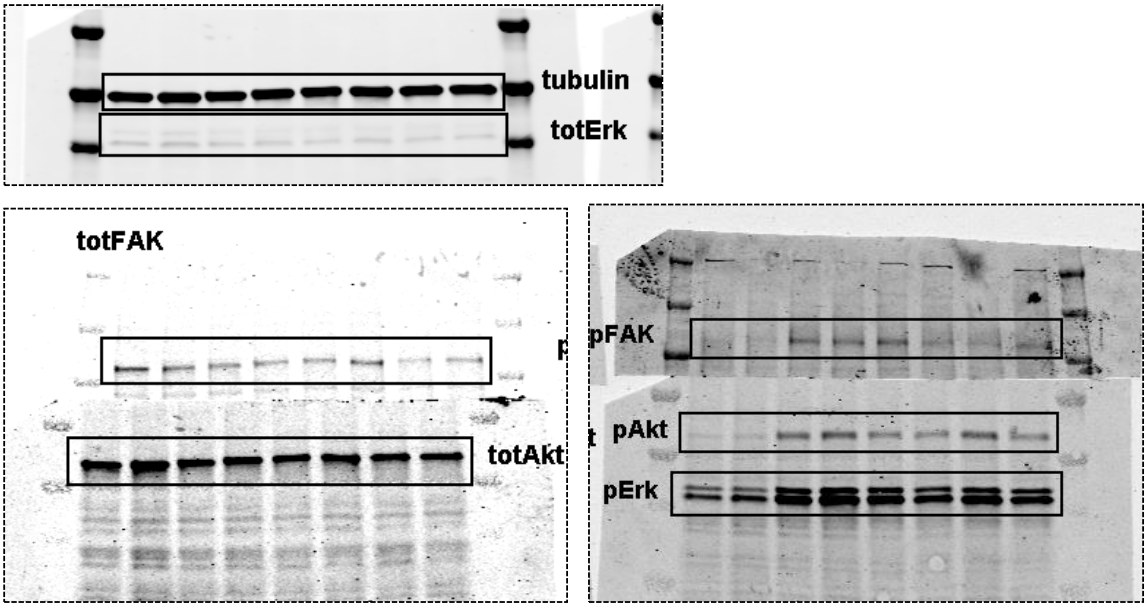

Supplementary Figure 4f.

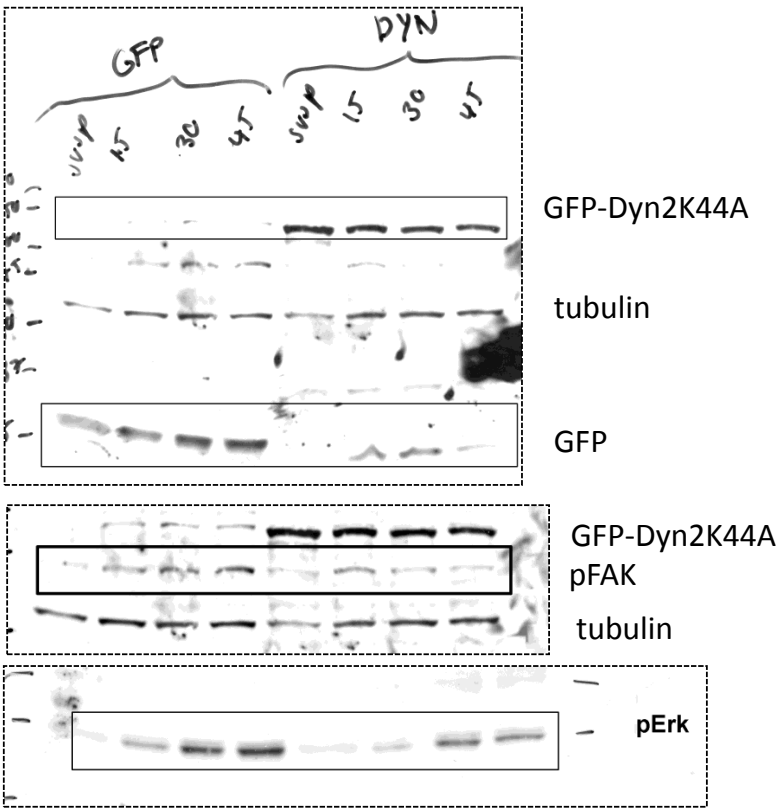

Supplementary Figure 9 continued

Supplementary Figure 4h.

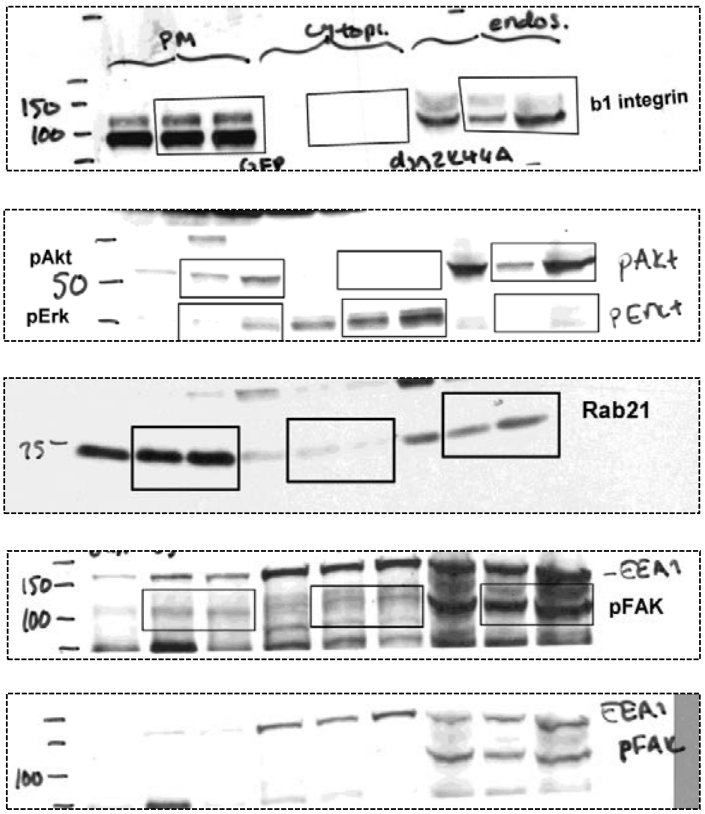

Supplementary Figure 4i.

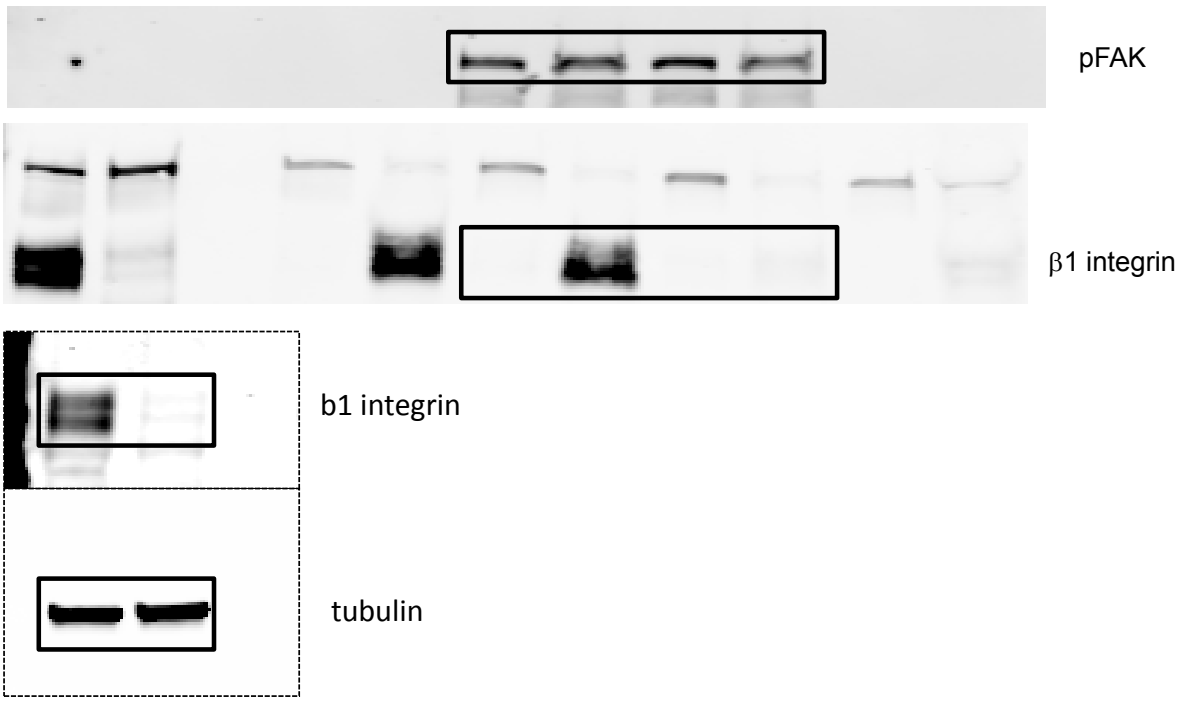

Supplementary Figure 9 continued

Supplementary Figure 4i. continues

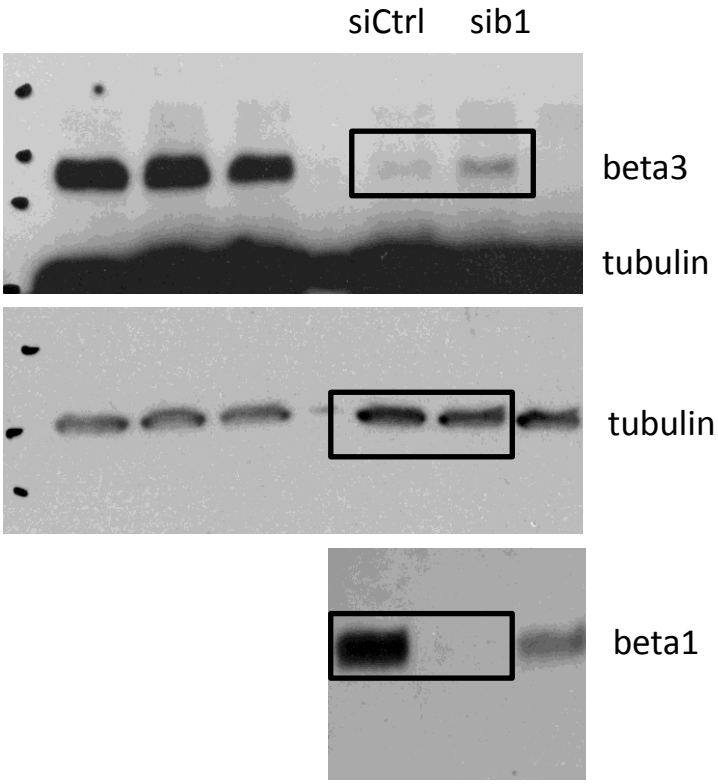

Supplementary Figure 5c.

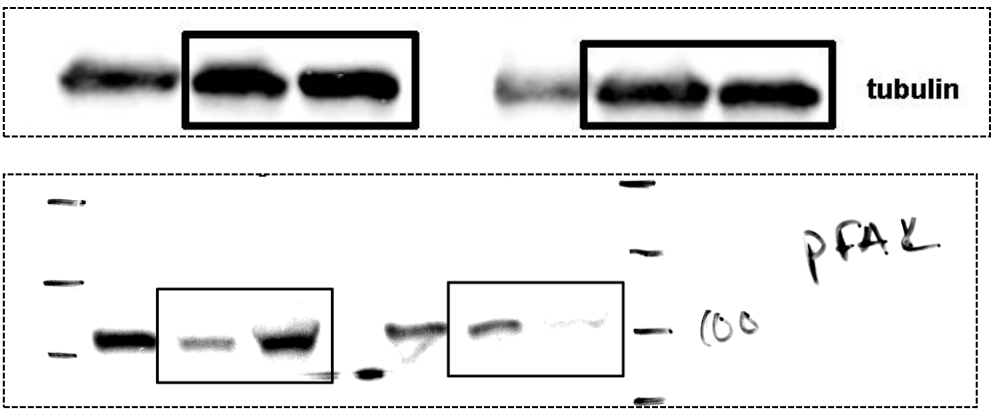

Supplementary Figure 9 continued

Supplementary Figure 6a.

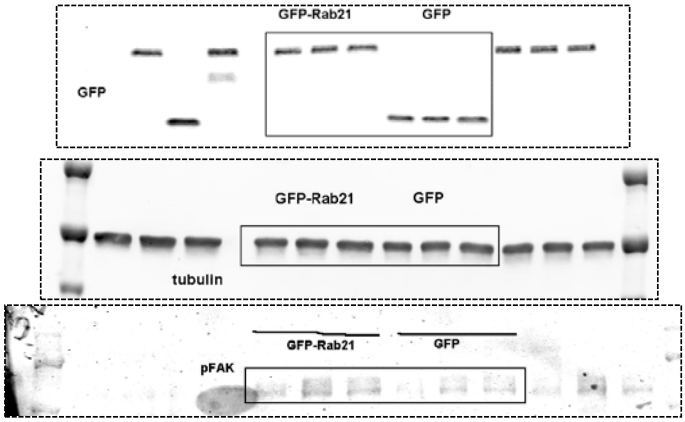

Supplementary Figure 6b.

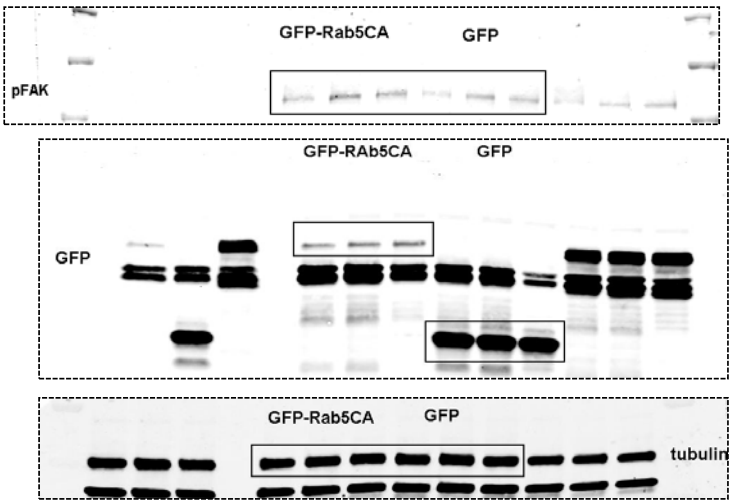

Supplementary Figure 6d.

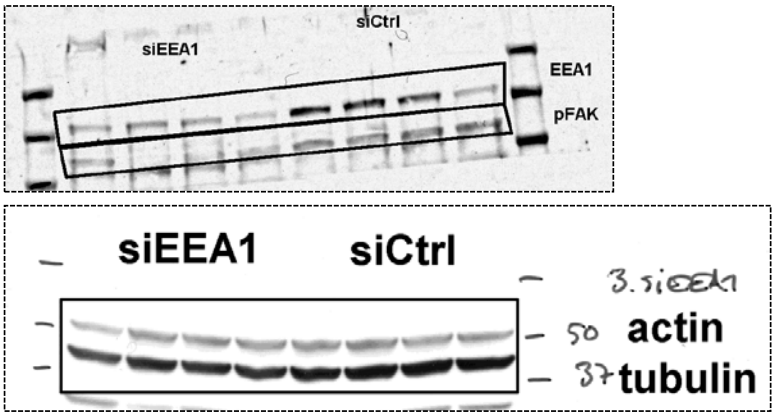

Supplementary Figure 9 continued

Supplementary Table Legends

Supplementary Table 1 Proteins identified from plasma membrane, endosomal and cytoplasmic fractions. Two biological replicate proteomic analyses (R1 and R2) of proteins isolated from mouse embryonic fibroblast cells were performed. The table shows all proteins identified following database searches using MASCOT and data validation using Scaffold. For each protein, the number of spectra identified from each replicate is shown as well as the normalised spectral counts (normalised to total number of IDs and molecular weight). In addition, column on the left indicate whether each identified proteins is part of the Geiger Adhesome (Zaidel-Bar R et al, 2010) or was previously identified in various MS analyses of adhesion complexes.

Supplementary Table 2 Statistics source data

Supplementary Table 3 List of antibodies and dilutions used in the study